# Molecular mechanisms associated with digenic inheritance of TRPS1 and IL6ST in craniosynostosis

**Yu, Jung Woo**

**Department of Medicine**

**Graduate School**

**Yonsei University**

# Molecular mechanisms associated with digenic inheritance of TRPS1 and IL6ST in craniosynostosis

**Advisor Lee, Min Goo**

**A Dissertation Submitted**
**to the Department of Medicine**
**and the Committee on Graduate School**
**of Yonsei University in Partial Fulfillment of the**
**Requirements for the Degree of**
**Doctor of Philosophy in Medical Science**

**Yu, Jung Woo**

**June 2025**

**Molecular mechanisms associated with digenic inheritance of TRPS1 and IL6ST in craniosynostosis**

**This Certifies that the Dissertation of Yu, Jung Woo is Approved**

| | |
|---|---|
| **Committee Chair** | Kim, Sangwoo |
| **Committee Member** | Shim, Kyu-Won |
| **Committee Member** | Lee, Min Goo |
| **Committee Member** | Gee, Heon Yung |
| **Committee Member** | Lee, Ji Hyun |

**Department of Medicine**
**Graduate School**
**Yonsei University**
**June 2025**

# ACKNOWLEDGEMENT

First, I would like to express my sincere gratitude to Kim Ji Sun and You Yi Jun for their unwavering support. My heartfelt thanks also go to my parents, You Jung Min, and Ha Seong hyeon.

Additionally, I am deeply thankful to Prof. Lee Min-gu for his patience and guidance throughout my studies, especially as a slow learner, helping me reach graduation. My appreciation extends to Noh Shin-hye and Han Chae-rim for their crucial assistance in completing my degree. I am also grateful to Prof. Jang Won-seok and Prof. Jung Hyun-ho for their continuous support of my research after I moved to the Neurosurgery Department, and to Han Sang-heon for his enjoyable conversations.

Finally, I will carry the efforts of my past during this doctoral program in my heart as I take my next steps into the future. Thank you.

# TABLE OF CONTENTS

# LIST OF FIGURES

# LIST OF TABLES

ABSTRACT

## Molecular mechanisms associated with digenic inheritance of TRPS1 and IL6ST in craniosynostosis

Craniosynostosis (CRS) is characterized by abnormal cranial suture ossification and premature fusion. Although several associated genetic disorders have been identified, the genetic determinants in CRS remain poorly understood. Using exome data from 121 CRS patients including 52 trios, we performed integrative analyses of ***de novo* variants, pathogenic variants, and oligogenic combinations** in haploinsufficient genes with rare variants. Our findings reveal that genes associated with CRS share a molecular network with genes linked to skeletal and neurodevelopmental disorders, with an enrichment of deleterious variants in haploinsufficient genes. We identified six unique digenic pairs in haploinsufficient genes specific to CRS patients. *In vitro* experiments validated the functional impact of the identified variants and demonstrated accelerated bone mineralization resulting from the digenic effects of *IL6ST* and *TRPS1* in osteoblast cells. Our study highlights the significant role of rare variants in haploinsufficient genes and expands the genetic spectrum of CRS to digenic or oligogenic inheritances in the CRS pathogenesis.

# 1. INTRODUCTION

The development of the human brain is intricately tied to the ossification process of cranial sutures. Premature fusion of these sutures gives rise to craniosynostosis (CRS), a pathological condition that not only alters the shape of the skull bone but also affects brain development, potentially leading to neurodevelopmental disorders (NDDs), such as intellectual disability[1]. CRS is widely acknowledged to have a significant genetic component, and while approximately one hundred genes have been identified as monogenic causes of CRS[2,3], most of these genetic defects have been identified in syndromic cases. Previous studies have highlighted the pronounced burden of *de novo* mutations within the WNT, BMP, and Ras/ERK signaling pathways in non-syndromic cases[4]. However, the genetic architecture of CRS, in particular that of non-syndromic CRS, remains poorly understood; and, moreover, the identified variants have occasionally exhibited weak phenotypic associations with incomplete penetrance.

Despite advancements in sequencing technologies that have facilitated genomic exploration, identifying the causative genes responsible for human traits within the context of Mendelian inheritance remains a challenge. In our recent investigation using the target sequencing panel for 34 CRS-related genes, we observed that individuals with rare or structural variations in causative genes accounted for up to 30% of CRS patients in a Korean cohort[5], including incomplete penetrance in the haploinsufficiency genes that are associated with autosomal dominant disorders, such as *ERF* and *TCF12*[6,7]. Recent studies have shed light on the oligogenic nature of various disorders, including congenital heart defects, microcephaly, and brain malformation[8-11]. In CRS, a previous study suggested a two-locus model for non-syndromic midline CRS involving interaction between *SMAD6* rare variants and a common *BMP2* allele[12]; however, this finding has been contradicted by another study[13]. Instead, a recent study shows that the digenic combinations of *IGF1* and *RUNX2* may contribute to the pathogenesis of CRS in mouse models[14]. Nevertheless, no comprehensive investigation has explored the digenic or oligogenic inheritance model for human CRS on a genome-wide scale.

The task of identifying the full spectrum of causative digenic or oligogenic pairs from the vast number of potential gene-gene interactions remains challenging, despite the development of computational tools to identify oligogenic combinations[15,16]. Herein, we examine the possibility that CRS could be attributed to the presence of two haploinsufficient genes acting in a digenic dominant mode. To accomplish this, we focused on haploinsufficient genes identified through gene constraint metrics, specifically the probability of loss of function intolerance (pLI), which was calculated based on a large human population[17]. Our choice of approach is supported by previous findings demonstrating the dosage effect of CRS-related genes in both humans[6,7] and mice[14], as well as the notable genetic effects observed from *de novo* or transmitted rare variants in the constrained genes[18]. Consequently, our objectives were to identify specific digenic combinations in CRS probands that harbored both deleterious rare variants and to delineate their biological contribution to the disease mechanism of CRS.

The initial analyses in this study, using exome sequencing data from 121 CRS probands comprising 52 trios and 69 proband-only samples, revealed the enrichment of deleterious variants in haploinsufficient genes associated with neurodevelopmental and skeletal disorders in patients with CRS. We subsequently focused on the 52 trios, in which we identified patient-specific digenic rare variant combinations in the haploinsufficient genes. Further analysis of 69 proband-only samples revealed the presence of the same digenic combinations in several cases. To gain insight into the biological relevance of these variants, we selected a pair of genes that are known to be involved in bone ossification[19], *TRPS1* and *IL6ST*, and conducted *in vitro* experiments to examine their effects on bone homeostasis.

# 2. MATERIALS AND METHODS

## 1. Patients

The patient cohort consisted of 121 unrelated Korean pediatric patients who were diagnosed with CRS (**Table 1**). Among 110 patients who underwent targeted gene panel assessment[5], 93 were enrolled for exome sequencing excluding definite monogenic causes

with complete penetrance such as *FGFR2*, *FGFR3*, *TWIST1*, and *EFNB1*. Of these, 79 cases remained unresolved after targeted sequencing for 34 CRS-related genes, and 14 cases with incomplete penetrance variants (*TCF12* [*n* = 4], *ERF* [*n* = 3], *ALPL* [*n* = 1], *FBN1* [*n* = 1]) or chromosomal abnormalities with unknown associations (1p32-p31 deletion [*n* = 1], 10q26 deletion [*n* = 1], 16p11.2 deletion [*n* = 2], 17p13.3 deletion [*n* = 1]) were included in this study. To supplement the initial patient cohort, an additional 28 new cases were enrolled for initial molecular evaluation between Aug 2017 and Sep 2019 at the Craniofacial Reforming and Reconstruction Clinic of Severance Hospital, Seoul, Republic of Korea. The overall diagnostic workup process has been previously described [5]. Informed consent was obtained from all participants or their parents. This study was conducted in accordance with the principles outlined in the Declaration of Helsinki and was approved by the local ethics committee (Yonsei University Health System 4-2015-0676). To serve as population controls, we included a group of 1,048 healthy Korean individuals from the Korean Genome Project (Korea1K) [20] who were matched based on their ancestry. Whole-genome sequencing (WGS) data were provided by the Korean Genomics Center at the Ulsan National Institute of Science and Technology (UNIST), and we applied the same quality control steps used in the study without requiring a minimum depth (DP ≥ 10).

## 2. Whole-exome sequencing and data processing

Peripheral blood samples were collected from a total of 225 participants, including 52 trio families and 69 proband-only samples. Genomic DNA (gDNA) was extracted from peripheral blood using the QIAamp DNA mini kit (Qiagen; Hilden, Germany) following the manufacturer's protocol. The concentration and purity of the extracted gDNA were assessed using a Nanodrop spectrophotometer (Thermo Fisher Scientific, MA, USA). A minimum of 500 ng of gDNA was used for the preparation of whole-exome sequencing libraries. We employed the xGen Exome Research Panel v1 (Integrated DNA Technologies, Inc., CA, USA) for targeted enrichment of exonic regions. The library preparation involved shearing the gDNA samples, followed by end-repair, A-tailing, adapter ligation, and PCR

amplification. The sequencing was carried out using the NovaSeq 6000 system (Illumina, CA, USA), generating paired-end reads of 150-bp in length. The average depth of coverage was 151x, and the percentage of target regions with above 20X stood at 96.3%.

Germline variant calling was conducted by following the Genome Analysis Tool Kit (GATK; https://gatk.broadinstitute.org/) Best Practices for germline short variant discovery, with modifications from the previous pipeline[5]. GATK (v4.1.4), Picard (v2.20.8), and Samtools (v1.9) were utilized, and reads were aligned to the human reference genome of GRCh37/hg19. A joint genotyping and genotype refinement workflow was implemented, followed by the application of a variant hard filter. The VQSR tranche was set at ≤ 99.7 for single-nucleotide variants (SNVs) and ≤ 99.0 for insertions and deletions (indels). Variants were excluded from further analysis if they had a genotype quality (GQ) < 20, a depth of coverage (DP) < 20, a missing genotype rate > 10%, or violated the Hardy-Weinberg equilibrium ($P < 10^{-12}$) or allelic balance ranges (0.3 < AB < 0.7 for heterozygotes, AB > 0.98 for homozygotes).

ANNOVAR (https://annovar.openbioinformatics.org/) was used for annotation with Ensemble, avsnp150, dbNSFP v4.2a[21], gnomAD v2.1.1[22], Online Mendelian Inheritance in Man (OMIM; https://omim.org/)[23], and InterVar[24] databases. All coding or nearby variants were classified into synonymous, missense, in-frame, frameshift, splice site, or nonsense variants. Specifically, we defined likely gene-disrupting (LGD) variants to include frameshift, nonsense, and splicing site (±5bp) variants that were predicted to be deleterious by dbscSNV (ADA > 0.9)[25]. Furthermore, we considered damaging missense (D-mis) variants with a DANN score above 0.98[26].

## 3. De novo variant analysis

*De novo* variants were analyzed in 52 proband-parent trios. To identify *de novo* variants, the trio samples were jointly analyzed with pedigree information, and the analysis followed stringent criteria with some modifications[18]. In brief, the candidate *de novo* variants were required to be heterozygous in probands and reference genotypes in both parents, and have

a population allele frequency of less than 0.1% in the gnomAD v.2.1.1 exome. Only high confidence sites with GQ ≥ 60, DP ≥ 20, and AB between 0.3 and 0.7 for probands and GQ ≥ 25, DP ≥ 20, and AB < 0.03 for both parents were included. To validate our findings, we performed *in silico* confirmation of *de novo* candidates using DeepVariant[27]. We only included variants with a PASS for further analysis. Finally, we analyzed confirmed *de novo* variants using the R package 'denovolyzeR' (http://denovolyzer.org/)[28]. The pathogenicity of each *de novo* variant was classified based on the American College of Medical Genetics and Genomics (ACMG)/Association for Molecular Pathology (AMP) criteria[29]

## 4. Digenic combinations in haploinsufficient genes

Haploinsufficient genes were identified based on a pLI score > 0.9, obtained from the Genome Aggregation Database (gnomAD) comprising 141,456 human genomes[17]. Genes located in sex chromosomes were excluded, resulting in a final set of 2,831 autosomal genes (chromosomes 1-22) for further analysis. To ensure reliable results, we utilized an exploratory and validation cohort consisting of 52 trios and 69 proband-only samples. Digenic combinations (Gene A × Gene B) with rare variants (minor allele frequency [MAF] < 0.5%) in haploinsufficient genes, specifically loss-of-function (LGD) or damaging missense (D-mis) variants, were prioritized. Using the 52 trios, we searched for all possible combinations, considering one allele from the father and one allele from the mother. Digenic pairs that also contained LGD or D-mis rare variants in the parents or population controls were excluded to minimize false-positive detections. Consequently, we extracted case-specific digenic combinations harboring LGD or D-mis rare variants. To assess the pathogenicity of these digenic combinations, we employed the Variant Combination Pathogenicity Predictor (VarCoPP) provided by the Oligogenic Resource for Variant Analysis (ORVAL)[15]. VarCoPP utilizes individual variant information to classify digenic combinations into four categories: "Neutral," "Candidate disease-causing," "99%-zone disease-causing," and "99.9%-zone disease-causing," based on the VarCoPP score. We focused exclusively on the predicted disease-causing combinations falling within the

99.9%-zone. Additionally, we considered genes with reported brain or skeletal expression in the Genotype-Tissue Expression (GTEx) portal (https://gtexportal.org/)[30]. To validate the selected digenic combinations, we analyzed the 69 proband-only samples. We sought to identify additional cases exhibiting the same digenic pairs. As a result of these procedures, we identified six digenic pairs that were uniquely observed in individuals with CRS in two or more independent cases (**Table 5**).

## 5. Dual-luciferase promoter activity assay

To investigate the functional activities of TRPS1 and IL6ST gene variants, we conducted *in vitro* experiments using a dual-luciferase Reporter Assay System (E1910, Promega, MW, USA). Plasmids encoding C-terminal DYK-tagged human TRPS1 (RC215856, OriGene, MD, USA) and IL6ST (RC215123, OriGene, MD, USA) were commercially purchased for this study. We generated TRPS1 (Q181R and R814L) and IL6ST (N360S and S580F) mutants from wild-type (WT) vectors using site-directed mutagenesis techniques. These mutants were used to assess the functional activities of the variants. To eliminate potential confounding effect of endogenous TRPS1 and IL6ST expression, we selected HepG2 and HEK293 cells for the assay, respectively (**Fig. 4**). HepG2 cells were plated and allowed to attach for 24 h prior to transfection, which was performed using TransIT-LT1 Transfection Reagent (MIR2300, Mirus Bio, MW, USA). We utilized the p6OSE2-luciferase vector (200 ng / 24 well) to measure the effect of TRPS1 on osteogenic-specific function. To assess the luciferase activity, we co-transfected the RUNX2 vector (250 ng / 24 well) with TRPS1 WT, Q181R, or R814L variants (30 ng / 24 well). For IL6ST variants, HEK293 cells were plated and allowed to attach for 24 h. To eliminate endogenous IL6ST expression, we employed IL6ST siRNA to silence its expression. The siRNA specifically targeted the 3'-untranslated region of IL6ST mRNA and was transfected using TransIT-LT1 Transfection Reagent. After 6 h, we transfected IL6ST variants (WT, N360S, and S580F) at a concentration of 200 ng / 24 well. We used pGL4.47 [luc2P/SIE/Hygro] (E4041, Promega, MW, USA), IL11RA (RC200654, OriGene, MD, USA), and pGL4.70 [hRluc] (E6881,

Promega, MW, USA) vectors to measure the activities of the IL6ST variants. Following transfection, the cells were maintained in a serum-free medium and stimulated with recombinant human IL-11 (1 ng/ml) (P20809, PeproTech, NJ, USA) for 6 h. Luciferase assay results were normalized by assessing Renilla luciferase activity and presented as Firefly/Renilla luciferase activity.

## 6. Double knockdown of TRPS1 and IL6ST in mouse osteoblast cells and osteoclast

To investigate the combined effects of TRPS1 and IL6ST on bone ossification, we performed a double knockdown experiment using MC3T3-E1 mouse osteoblast cells (ATCC CRL-2593). The cells were cultured in 12-well plates using alpha-minimum essential medium (a-MEM) without L-ascorbic acid (LM008-53, Welgene), supplemented with 10% fetal bovine serum (26140-079, Gibco), and Penicillin/Streptomycin (15140-122, Gibco) during the cell proliferation phase. During the differentiation phase, the culture medium was supplemented with 50 μg/ml L-ascorbic acid (A4544, Sigma) and 10 mM β-glycerophosphate (G9422, Sigma), and were replaced every 3 days. After the MC3T3-E1 cells were plated in a 12-well plate for 16-24 h, siRNAs targeting TRPS1 and IL6ST (**Table 2**) were transfected into the cells using Lipofectamine RNAiMAX (13778-100, Invitrogen) as per the manufacturer's protocol. The cells were allowed to grow and stabilize for 48 h after transfection to ensure proper cell growth and environment. Osteogenic induction medium was then added and replaced every 3 days. After day 5~7 of osteogenic induction, the cells were extracted from the wells using Tri-RNA Reagent (FATRR001, FAVORGEN), and the resulting cell lysates were used for the ALP assay and qRT-PCR.

To investigate the roles of TRPS1 and IL6ST in osteoclasts, we utilized the RAW264.7 cell line (ATCC TIB-71). The cells were seeded in 24-well plates using a-MEM (LM008-01, Welgene), supplemented with 10% fetal bovine serum and Penicillin/Streptomycin. After seeding for 16-24 h, siRNAs targeting TRPS1 and IL6ST (**Table 2**) were transfected into the cells using TransIT-LT1 Transfection Reagent. After 24 h, to induce osteoclast

differentiation, 100 ng/ml RANKL (315-11, PeproTech, NJ, USA) was added to the cells every day. For qRT-PCR, the cells were extracted day 3 after the start of differentiation. After day 5 of differentiation, TRAP staining was performed.

## 7. ALP assay, staining, and quantitative RT-PCR

To measure the ossification of osteoblasts, we used the ALP assay kit (ab83369, Abcam) following the manufacturer's protocol. In brief, cell lysates were collected from the ALP assay buffer in 12-well plates, and p-nitrophenyl phosphate (pNPP) solution was added to 96-well plates. After adding the pNPP solution to each well, the plates were incubated in the dark for 1 h. The ALP activities were measured based on colorimetric changes using an ELISA reader. For ALP staining, we used the ALP staining kit (294-67001, Wako). After day 5 ~ 7 of osteoblast differentiation, the culture medium in each well was removed and washed using D-PBS (LB001-02, Welgene). Each well was then treated with formaldehyde for 10 min in an icebox, fixed by alcohol/acetone, and the ALP staining solution was added. After 15 min, ALP staining was visually confirmed.

To extract cell lysates, we used the Tri-RNA Reagent. Total RNA was isolated from the cell lysates using the RNA extraction kit (K-3140, Bioneer) in accordance with the manufacturer's instructions. RNA to cDNA conversion was performed using the EcoDry Premix (639549, TaKaRa) following the recommended protocol. To assess the knockdown efficiency of the target genes (TRPS1 and IL6ST) after 48 h of transfection, qRT-PCR was performed. Additionally, after day 7 of osteoblast differentiation, bone formation markers (IBSP, BGLAP1, COL1A1, RUNX2, ALPL) were analyzed to check differentiation. The primer information for each gene is provided in **Table 2**.

## 8. TRAP staining, multi-nucleated cell count and quantitative RT-PCR

TRAP staining was performed using the TRAP staining kit (294-67001, Wako). After day 5 of osteoclast differentiation, the culture medium in each well was removed and washed with D-PBS (LB001-02, Welgene), following the same preparation process as described

above for ALP staining. The TRAP staining solution was added, and the staining was allowed to proceed for 15 min. To quantify the TRAP staining, multi-nucleated cells were counted, with multinucleated cells defined as those containing 5 or more nuclei. The number of counts was converted to percentages based on the scrambled group. To assess the knockdown efficiency of the target genes (TRPS1 and IL6ST) after 24 h of transfection, qRT-PCR was performed. Furthermore, after day 3 of osteoclast differentiation, osteoclast markers (CTSK, DCSTAMP, TRAP, and NFATc1) were analyzed to assess differentiation using qRT-PCR. The primer information for each gene is provided in **Table 2**.

## 9. Western blot

To perform Western blot analysis, MC3T3E1 cells were cultured in 12-well plates and washed twice with D-PBS. The cells were then scraped in Pierce RIPA buffer (89900, Thermo Scientific) and incubated for 6 h in osteogenic induction medium. Following incubation, the lysates were sonicated for 20 sec and centrifuged at 13,200 x g for 15 min at 4℃. The protein concentration of the resulting supernatants was determined using a BCA Protein assay kit (T9300A, TaKaRa). Equal amounts of protein were loaded onto a 10% SDS-PAGE gel and subsequently transferred to a nitrocellulose membrane (10600004, Amersham). To minimize nonspecific binding, the membrane was blocked with either 5% skim milk or 5% BSA in TBS buffer for 1 h at room temperature. Subsequently, the membrane was incubated overnight with primary monoclonal antibodies. Following the washing process, the membrane was incubated with a secondary monoclonal antibody, and the protein bands were visualized using a film. The intensity of the protein bands was quantified using the Densitometry program (Multi Gauge V3.0, Fujifilm).

## 10. Structural modeling

The AlphaFold Protein Structure Database was used to retrieve the predicted protein structure of *TRPS1* (UniProt: Q9UHF7) and *IL6ST* (UniProt: P40189)[31]. The PyMOL program (v. 2.5.5; PyMOL Molecular Graphics System, Schrödinger Inc., New York, NY,

USA) was used to visualize the figures.

## 11. Statistical analysis

Statistical analyses were performed using the software R (version 4.1.2). A *P*-value < 0.05 was considered significant. Data were analyzed using the Mann-Whitney U test or one-way analysis of variance (ANOVA) followed by Tukey's multiple comparison test, as appropriate.

**Table 1. Characteristics of 121 craniosynostosis patients enrolled in this study.**

| **Characteristics** | | ***n*** | **%** |
|---|---|---|---|
| Age | month, median [range] | 15 | [2-120] |
| Sex | | | |
| | Male | 74 | 61.2% |
| | Female | 47 | 38.8% |
| Exome sequencing | | | |
| | Trio | 52 | 43.0% |
| | Proband only | 69 | 57.0% |
| Molecular assessment | | | |
| | Targeted sequencing for 34 CRS genes | 93 | 76.9% |
| | Unsolved cases | 79 | 65.3% |
| | Prior diagnosis[a] | 14 | 11.6% |
| | No prior molecular work-up | 28 | 23.1% |
| Clinical features | | | |
| | Syndromic | 44 | 36.4% |
| | Non-syndromic | 77 | 63.6% |
| Cranial suture involvement | | | |
| | Metopic (M) | 9 | 7.4% |
| | Sagittal (S) | 43 | 35.5% |
| | Coronal (C) | 34 | 28.1% |
| | Lambdoid (L) | 16 | 13.2% |
| | Multiple | 19 | 15.7% |

[a]Cases with chromosomal abnormalities, including 1p32-p31 deletion (*n* = 1), 10q26 deletion (*n* = 1), 16p11.2 deletion (*n* = 2), 17p13.3 deletion (*n* = 1), and incomplete penetrance genes, including *TCF12* (*n* = 4), *ERF* (*n* = 3), *ALPL* (*n* = 1), *FBN1* (*n* = 1), were enrolled

**Table 2. The list of sequences.**

| Name | F/R | Sequence |
|---|---|---|
| **RT-PCR** | | |
| GAPDH | F | 5'-CATCACTGCCACCCAGAAGACTG-3' |
| | R | 5'-ATGCCAGTGAGCTTCCCGTTCAG-3' |
| IL6ST | F | 5'-CTCTGAGTCCTTGAAGGCGTAC-3' |
| | R | 5'-CCATTCTGGTCGTCCACAGGAA-3' |
| TRPS1 | F | 5'-CAACCGTTCTGTGCTTTCTGGC-3' |
| | R | 5'-GTGTTGCCTTGGCAATCTGGAG-3' |
| IBSP | F | 5'-AATGGAGACGGCGATAGTTCCG-3' |
| | R | 5'-GGAAAGTGTGGAGTTCTCTGCC-3' |
| BGLAP1 | F | 5'-GCAATAAGGTAGTGAACAGACTCC-3' |
| | R | 5'-CCATAGATGCGTTTGTAGGCGG-3' |
| Col1A1 | F | 5'-CCTCAGGGTATTGCTGGACAAC-3' |
| | R | 5'-CAGAAGGACCTTGTTTGCCAGG-3' |
| RUNX2 | F | 5'-CCTGAACTCTGCACCAAGTCCT-3' |
| | R | 5'-TCATCTGGCTCAGATAGGAGGG-3' |
| ALPL | F | 5'-CCAGAAAGACACCTTGACTGTGG-3' |
| | R | 5'-TCTTGTCCGTGTCGCTCACCAT-3' |
| CTSK | F | 5'-AGCAGAACGGAGGCATTGACTC-3' |
| | R | 5'-CCCTCTGCATTTAGCTGCCTTTG-3' |
| DCSTAMP | F | 5'-TTTGCCGCTGTGGACTATCTGC-3' |
| | R | 5'-GCAGAATCATGGACGACTCCTTG-3' |
| TRAP | F | 5'-GCGACCATTGTTAGCCACATACG-3' |
| | R | 5'-CGTTGATGTCGCACAGAGGGAT-3' |
| NFATc1 | F | 5'-GGTGCCTTTTGCGAGCAGTATC-3' |
| | R | 5'-CGTATGGACCAGAATGTGACGG-3' |
| **siRNA** | | |
| siIL6ST | F | 5'-CUGCUUAUUCUGUAGUGAAdtdt-3' |
| | R | 5'-UUCACUACAGAAUAAGCAGdtdt-3' |
| | F | 5'-GUGCUAUCAAAUCACAGUAdtdt-3' |

| | | |
|---|---|---|
| siTRPS1 | R | 5'-UACUGUGAUUUGAUAGCACdtdt-3' |
| | F | 5'-CUCGAACUUCCUUCACUGUdtdt-3' |
| | R | 5'-ACAGUGAAGGAAGUUCGAGdtdt-3' |
| | F | 5'-CUCAUGUGUUUCUGAUCAUdtdt-3' |
| | R | 5'-AUGAUCAGAAACACAUGAGdtdt-3' |
| | F | 5'-CUGCUAAACCCAGACUCUAdtdt-3' |
| | R | 5'-UAGAGUCUGGGUUUAGCAGdtdt-3' |
| | F | 5'-CUGCAAUAGGUUGUCUACAdtdt-3' |
| | R | 5'-UGUAGACAACCUAUUGCAGdtdt-3' |
| siIL6ST(3'-UTR) | F | 5'-GAUGUUUGCACUGAAGAAAdtdt-3' |
| | R | 5'-UUUCUUCAGUGCAAACAUCdtdt-3' |
| **Site-directed mutagenesis** | | |
| TRPS1_Q181R | F | 5'-ATTGGCTTGACCACTCCGTGCTTGCCCTGTTTC-3' |
| | R | 5'-GAAACAGGGCAAGCACGGAGTGGTCAAGCCAAT-3' |
| TRPS1_R814L | F | 5'-TGACGGACTCCCCAGCAGGATGTCTGC-3' |
| | R | 5'-GCAGACATCCTGCTGGGGAGTCCGTCA-3' |
| IL6ST_N360S | F | 5'-TCCAAGATTTTTCCACTGGCTTCAAAAGGAGGCAATGTC-3' |
| | R | 5'-GACATTGCCTCCTTTTGAAGCCAGTGGAAAAATCTTGGA-3' |
| IL6ST_S580F | F | 5'AATGTGTCACTAGTCAAAGAGAACAATGTATATTCTGTGTGGG-3' |
| | R | 5'CCCACACAGAATATACATTGTTCTCTTTGACTAGTGACACATT-3' |
| **Patient genotyping** | | |
| TRPS1_Q181R | F | 5'-TCAAGATATGGCCTGCACCCCCTC-3' |
| | R | 5'-TTTGGATTTATTCAGTCTTACACCCCCA-3' |
| TRPS1_R814L | F | 5'-CCACCATCAAAGAGGAGCCCAAAAT-3' |
| | R | 5'-CACAGCCAAGCCATAAATAGGTCGC-3' |
| IL6ST_N360S | F | 5'-GCGATCATTTGTGAGATTTACTGTCAGTTTTGTG-3' |
| | R | 5'-GACATAATGGCATGATTTGTGAATATGAAG-3' |
| IL6ST_S580F | F | 5'-TTCTGGACCATCCTTCCCACCTTC-3' |
| | R | 5'-CTTCCAGCTGTGAATGTGGATTCTTCCC-3' |

# 3. RESULTS

## 1. Molecular profiling of CRS patients using exome sequencing

This study included a total of 121 unrelated Korean patients with CRS, comprising twenty-eight newly enrolled individuals (23.1%) and ninety-three (76.9%) for whom definitive causative genes had not been identified in a previous targeted gene panel sequencing[5] (**Table 1**). The male gender was more prevalent, accounting for 59.5% of all cases; and non-syndromic cases ($n$ = 77, 63.6%) were more common than syndromic ones ($n$ = 44, 36.4%). We performed whole-exome sequencing (WES) on 52 trios (patient and both parents) and 69 proband-only samples (patients without available parental samples; **Fig. 1A**). For ancestry-matched controls, we utilized whole-genome sequencing (WGS) data from 1,048 healthy Korean individuals obtained from the Korean Genome Project[20]. The majority of CRS cases (84.3% [$n$ = 102]) exhibited involvement of a single cranial suture, specifically with 43 sagittal, 34 coronal, 16 lambdoid, and 9 metopic sutures affected (**Fig. 1B**). None of the patients had a family history of CRS.

First, we focused on analyzing *de novo* variants in the 52 trios and identified a total of 80 *de novo* variants in protein-coding regions or nearby junctions (**Fig. 1C**). These variants consisted of 76 single nucleotide variants (SNVs) and 4 small insertions or deletions (indels). The transition-to-transversion (Ti/Tv) ratio for *de novo* SNVs was calculated as 2.45.

In our investigation, we identified 65 protein-altering variants (missense and likely gene disrupting [LGD]) in 62 genes, which were further classified into three categories: CRS-, NDD-, and unknown-associated genes. Pathway analysis of these genes highlighted their involvement in biological pathways related to neurogenesis, neuron differentiation, and cranial suture abnormalities (**Fig. 2**). Among these genes, 26 were previously associated with CRS or NDDs. Furthermore, when comparing the characteristics of genes in the CRS/NDD and the unknown categories, we found that CRS/NDD genes exhibited higher pLI scores (median 0.64 vs. 0.026, $P$ = 0.046) and had higher deleterious *in silico*

predictions (median DANN_rank score 0.741 vs. 0.463, $P$ = 0.0094) than the unknown genes (**Fig. 1D**). These results suggest that genes contributing to CRS phenotypes are more likely to harbor deleterious variants in haploinsufficient genes.

Subsequently, we investigated rare variants that could be associated with Mendelian disorders. Our analysis unveiled 16 *de novo* variants, classified as pathogenic (P) or likely pathogenic (LP), which were linked to dominant disorders in 26.9% of the trio probands (14/52, **Table 3**). While some variants were found in well-known CRS genes such as *FGFR2*, *TCF12*, *EFNB1*, and *SKI*, we also identified P/LP variants in genes associated with NDDs and skeletal disorders, such as *NF1*, *RERE*, *COL9A2*, *TAOK1*, *RTEL1*, *TGFBR1*, *MTOR*, *KMT2D*, and *TANC2* (**Table 4**). Pathway analysis of the 40 genes highlighted their involvement in biological pathways related to neuron and osteoblast differentiation, and bone ossification (**Fig. 2C,D**). These findings highlight the close relationship between CRS and the molecular networks underlying NDDs and skeletal disorders, and potentially implicate the manifestation of CRS as a phenocopy or a phenotypic expansion of one or both of these types of disorders.

**Table 3. Pathogenic or likely pathogenic *de novo* variants identified in the 52 trios with craniosynostosis.**

| Proband | Sex | Gene (Transcript) | HGVS variant | ACMG_criteria | OMIM | CRS | Other clinical features |
|---|---|---|---|---|---|---|---|
| P024 | male | *NF1* (NM_001042492.3) | c.3103A>G, p.(M1035V) | PS2, PM1, PM2, PP3 (LP) | Watson syndrome, AD (#193520) | S, M | No |
| P028 | male | *RERE* (NM_001042681.2) | c.1978G>A, p.(E660K) | PS2, PM2, PP3 (LP) | Neurodevelopmental disorder with or without anomalies of the brain, eye, or heart, AD (#616975) | BC | No |
| P038 | male | *COL9A2* (NM_001852.4) | c.1298G>C, p.(G433A) | PS2, PM2, PP3 (LP) | Epiphyseal dysplasia, multiple, 2, AD (# 600204) | BC | IUGR, necrotizing enterocolitis, hemorrhagic hydrocephalus, ankyloglossia |
| P042 | male | *TAOK1* (NM_020791.4) | c.2545-1_2545insT, p.(I849Yfs*2) | PVS1, PS2, PM2 (P) | Developmental delay with or without intellectual impairment or behavioral abnormalities, AD (#619575) | LL | Development delay, preauricular skin tags |
| P058 | female | *TCF12* (NM_207037.2) | c.627del, p.(S210Vfs*35) | PVS1, PS2, PM2 (P) | Craniosynostosis 3, AD (#615314) | RC | Low set ears, preauricular fistula, high palate, short 5th fingers, leg length (Rt> Lt) |
| P116 | male | *RTEL1* (NM_032957.5) | c.919+5G>A | PS2, PM2, PP3 (LP) | Dyskeratosis congenita, AD 4 (#615190) | LL | Encephalocele enplaque, congenital preauricular fistula, short frenulum |
| P120 | female | *EFNB1* (NM_004429.5) | c.406+3G>T | PS2, PM2, PP3 (LP) | Craniofrontonasal dysplasia, XD (#304110) | LC | Hypertelorism, facial asymmetry, flat nose |
| P123 | male | *TGFBR1* (NM_004612.4) | c.944A>G, p.(H315R) | PS2, PM2, PP3, PP5 (LP) | Loeys-Dietz syndrome 1, AD (#609192) | S | Prominent forehead, flat nasal bridge, left inguinal hernia |
| P125 | female | *MTOR* (NM_004958.4) | c.1352A>G, p.(Y451C) | PS2, PM2, PP3 (LP) | Smith-Kingsmore syndrome, AD (#616638) | LL | No |

| | | | | | | | |
|---|---|---|---|---|---|---|---|
| P127 | male | *KMT2D* (NM_003482.4) | c.6109+3A>G | PS2, PM2, PP3 (LP) | Kabuki syndrome 1, AD (#147920) | LL | Rt. inguinal hernia |
| P128 | male | *FGFR2* (NM_000141.5) | c.1040C>G, p.(S347C) | PS2, PM1, PM2, PP3, PP5 (P) | Crouzon syndrome, AD (#123500) | BC, LL | Hydrocephalus, broad forehead, hypertelorism, large anterior fontanelle, downslant palpebral fissures, protoptosis, both, high palate |
| P130 | female | *SKI (NM_003036.4)* | c.107C>T, p.(A36V) c.374A>T, p.(Q125L) | PS2, PM1, PM2 (LP) PS2, PM2, PP3 (LP) | Shprintzen-Goldberg syndrome, AD (#182212) | S, BL | Hydrocephalus |
| P131 | male | *FGFR2* (NM_000141.5) | c.755C>G, p.(S252W) | PS2, PM1, PM2, PP3, PP5 (P) | Crouzon syndrome, AD (#123500) | BC | Prematurity, mild ventriculomegaly left, prominent forehead, polysyndactyly, single umbilical artery, hydronephrosis, dysmorphic cerebellum, atrial septal defect |
| P136 | male | *FGFR2* (NM_000141.5) | c.1025G>C, p.(C342S) | PS2, PM1, PM2, PP3, PP5 (P) | Crouzon syndrome, AD (#123500) | Pan | PDA, Type1 DM, atrial septal defect, Hypertelorism, Facial asymmetry |
| P140 | female | *TANC2 (NM_025185.4)* | c.4234G>A, p.(E1412K) | PS2, PM2, PP3 (LP) | Intellectual developmental disorder with autistic features and language delay, with or without seizures, AD (#618906) | S, BL | No |

Abbreviation: HGVS, Human Genome Variation Society; ACMG, American College of Medical Genetics and Genomics; P, pathogenic; LP, likely pathogenic; OMIM, Online Mendelian Inheritance in Men; AD, autosomal dominant; AR, autosomal recessive; XD, X-linked dominant; CRS, cranial suture involvement; S, sagittal; M, metopic; BC, bicoronal; RC, right coronal; LC, left coronal, BL, bilateral lambdoidal; LL, left lambdoidal; Pan, pansynostosis

**Table 4. The list of likely pathogenic or pathogenic variants associated with craniosynostosis identified in this study.**

| Sample | Chr:Pos:Ref:Alt (hg19) | Gene | CDS change | AA change | GT | Origin | MOI | OMIM_Pheno | OMIM_ID | Previously reported |
|---|---|---|---|---|---|---|---|---|---|---|
| P005 | chr19:42754483:C:T | *ERF* | c.257G>A | p.R86H | Het | Pat | AD | Craniosynostosis 4 | 600775 | Yes |
| P007 | chr4:1806119:G:A | *FGFR3* | c.1144G>A | p.G382R | Het | NA | AD | Muenke syndrome | 602849 | No |
| P023 | chr1:21894616:G:A | *ALPL* | c.437G>A | p.R146Q | Het | Mat | AR, AD | Odontohypophosphatasia | 146300 | Yes |
| P024 | chr17:29557390:A:G | *NF1* | c.3103A>G | p.M1035V | Het | De Novo | AD | Watson syndrome | 193520 | No |
| P025 | chr2:189859047:C:T | *COL3A1* | c.1282C>T | p.R428X | Het | NA | AD | Ehlers-Danlos syndrome, vascular type | 130050 | No |
| P028 | chr1:8421861:C:T | *RERE* | c.316G>A | p.E106K | Het | De Novo | AD | Neurodevelopmental disorder with or without anomalies of the brain, eye, or heart | 616975 | No |
| P028 | chr15:67073486:G:- | *SMAD6* | c.1104delG | p.G369Afs*170 | Het | Pat | AD | [32] | 617439 | No |
| P036 | chr3:151129114:C:T | *MED12L* | c.5854C>T | p.Q1952X | Het | NA | AD | Nizon-Isidor syndrome | 618872 | No |
| P038 | chr1:40769761:C:G | *COL9A2* | c.1298G>C | p.G433A | Het | De Novo | AD | Epiphyseal dysplasia, multiple, 2 | 600204 | No |
| P041 | chr19:18271883:G:- | *PIK3R2* | c.486delG | p.D163Ifs*24 | Het | Pat | AD | Megalencephaly-polymicrogyria-polydactyly-hydrocephalus syndrome 1 | 603387 | No |
| P042 | chr17:27869579:-:T | *TAOK1* | c.2102dupT | p.E702* | Het | De Novo | AD | Developmental delay with or without intellectual impairment or behavioral abnormalities | 619575 | No |
| P050 | chr7:19156550:C:G | *TWIST1* | c.395G>C | p.R132P | Het | NA | AD | Craniosynostosis 1 | 123100 | No |
| P052 | chr15:57565256:C:T | *TCF12* | c.1774C>T | p.P592S | Het | NA | AD | Craniosynostosis 3 | 615314 | Yes |
| P052 | chr7:151875096:-:T | *KMT2C* | c.7443-1->A | NA | Het | NA | AD | Kleefstra syndrome 2 | 617768 | No |
| P055 | chr19:54395039:C:T | *PRKCG* | c.641C>T | p.T214M | Het | De Novo | AD | Spinocerebellar ataxia 14 | 605361 | No |
| P057 | chr20:9416297:T:G | *PLCB4* | c.2613+2T>G | NA | Het | NA | AD, AR | Auriculocondylar syndrome 2 | 614669 | No |
| P058 | chr15:57523397:T:- | *TCF12* | c.627delT | p.S210Vfs*35 | Het | De Novo | AD | Craniosynostosis 3 | 615314 | Yes |
| P059 | chr14:77493815:T:- | *IRF2BPL* | c.321delA | p.Q107Hfs*45 | Het | Mat | AD | Neurodevelopmental disorder with regression, abnormal movements, loss | 618088 | No |

| | | | | | | | | | | |
|---|---|---|---|---|---|---|---|---|---|---|
| | | | | | | | | of speech, and seizures | | |
| P068 | chr15:57554285:A:G | *TCF12* | c.1468-7A>G | splicing | Het | NA | AD | Craniosynostosis 3 | 615314 | Yes |
| P069 | chr7:101917582:G:A | *CUX1* | c.1444+1G>A | NA | Het | NA | AD | Global developmental delay with or without impaired intellectual development | 618330 | No |
| P070 | chr15:48780645:T:C | *FBN1* | c.3128A>G | p.K1043R | Het | NA | AD | Geleophysic dysplasia 2 | 614185 | Yes |
| P070 | chr20:10629196:C:T | *JAG1* | c.1569+1G>A | NA | Het | NA | AD | Alagille syndrome 1 | 118450 | No |
| P070 | chr6:26104365:G:T | *H4C3* | c.190G>T | p.E64X | Het | NA | AD | Tessadori-Bicknell-van Haaften neurodevelopmental syndrome 1 | 619758 | No |
| P071 | chr12:49420288:C:T | *KMT2D* | c.15461G>A | p.R5154Q | Het | NA | AD | Kabuki syndrome 1 | 147920 | No |
| P074 | chr4:88537333:T:- | *DSPP* | c.3519delT | p.D1173Efs*141 | Het | Pat | AD | Dentinogenesis imperfecta | 125500 | No |
| P074 | chr9:101235538:C:- | *GABBR2* | c.889delG | p.A297Pfs*26 | Het | Mat | AD | Neurodevelopmental disorder with poor language and loss of hand skills | 617903 | No |
| P079 | chr11:65998371:C:- | *PACS1* | c.194delC | p.D66Tfs*40 | Het | NA | AD | Schuurs-Hoeijmakers syndrome | 615009 | No |
| P079 | chr4:2820024:C:- | *SH3BP2* | c.74delC | p.G27Dfs*43 | Het | NA | AD | Cherubism | 118400 | No |
| P088 | chr19:42753378:C:T | *ERF* | c.886G>A | p.G296S | Het | NA | AD | Craniosynostosis 4 | 600775 | Yes |
| P091 | chr12:32875561:C:T | *DNM1L* | c.464C>T | p.S155L | Het | De Novo | AR, AD | Encephalopathy, lethal, due to defective mitochondrial peroxisomal fission 1 | 614388 | No |
| P098 | chr19:42753237:GGGGCTGGGGCACCACCAGCCCAGGGTAGTGCAGGAAGGCGCG:- | *ERF* | c.985_1027del | p.R329Sfs*54 | Het | NA | AD | Craniosynostosis 4 | 600775 | Yes |
| P103 | chr12:122243911:GG:- | *SETD1B* | c.444_445del | p.K148Nfs*42 | Het | NA | AD | Intellectual developmental disorder with seizures and language delay | 619000 | No |
| P112 | chrX:67333079:T:- | *OPHN1* | c.1364delA | p.N455Ifs*7 | Hemi | Mat | XR | Intellectual developmental disorder, X-linked syndromic, | 300486 | No |
| P114 | chr7:19156479:T:C | *TWIST1* | c.466A>G | p.I156V | Het | NA | AD | Billuart type Craniosynostosis 1 | 123100 | Yes |
| P115 | chr7:114271592:C:T | *FOXP2* | c.151C>T | p.Q51X | Het | NA | AD | Speech-language disorder-1 | 602081 | No |
| P116 | chr20:62305451:G:A | *RTEL1* | c.919+5G>A | splice | Het | De Novo | AD | Dyskeratosis congenita, | 615190 | No |

| | | | | | | | | | | |
|---|---|---|---|---|---|---|---|---|---|---|
| P118 | chr15:57524504:C:- | *TCF12* | c.191delC | p.S64Ffs*11 | Het | NA | AD | autosomal dominant 4 Craniosynostosis 3 | 615314 | No |
| P119 | chr11:58919775:TG:- | *FAM111A* | c.634_635del | p.V213Lfs*25 | Het | Mat | AD | Gracile bone dysplasia | 602361 | No |
| P120 | chrX:68058740:G:T | *EFNB1* | c.406+3G>T | splice | Het | De Novo | XD | Craniofrontonasal dysplasia | 304110 | No |
| P121 | chr19:42754492:C:T | *ERF* | c.248G>A | p.R83Q | Het | Mat | AD | Craniosynostosis 4 | 600775 | No |
| P123 | chr9:101904956:A:G | *TGFBR1* | c.713A>G | p.H238R | Het | De Novo | AD | Loeys-Dietz syndrome 1 | 609192 | No |
| P125 | chr1:11303231:T:C | *MTOR* | c.1352A>G | p.Y451C | Het | De Novo | AD | Smith-Kingsmore syndrome | 616638 | No |
| P126 | chr15:57565399:AAAA:- | *TCF12* | c.747_750del | p.K250Sfs*14 | Het | Pat | AD | Craniosynostosis 3 | 615314 | No |
| P127 | chr12:49435869:T:C | *KMT2D* | c.6109+3A>G | splice | Het | De Novo | AD | Kabuki syndrome 1 | 147920 | No |
| P128 | chr10:123276877:G:C | *FGFR2* | c.695C>G | p.S232C | Het | De Novo | AD | Crouzon syndrome | 123500 | No |
| P130 | chr1:2160312:C:T | *SKI* | c.107C>T | p.A36V | Het | De Novo | AD | Shprintzen-Goldberg syndrome | 182212 | No |
| P130 | chr1:2160579:A:T | *SKI* | c.374A>T | p.Q125L | Het | De Novo | AD | Shprintzen-Goldberg syndrome | 182212 | No |
| P131 | chr10:123279677:G:C | *FGFR2* | c.410C>G | p.S137W | Het | De Novo | AD | Crouzon syndrome | 123500 | No |
| P135 | chr13:20605475:C:A | *ZMYM2* | c.1868C>A | p.S623X | Het | NA | AD | Neurodevelopmental-craniofacial syndrome with variable renal and cardiac abnormalities | 619522 | No |
| P136 | chr10:123276892:C:G | *FGFR2* | c.680G>C | p.C227S | Het | De Novo | AD | Crouzon syndrome | 123500 | No |
| P139 | chrX:128710001:G:A | *OCRL* | c.1841G>A | p.W614X | Hemi | NA | XR | Dent disease 2 | 300555 | No |
| P140 | chr17:61497577:G:A | *TANC2* | c.4234G>A | p.E1412K | Het | De Novo | AD | Intellectual developmental disorder with autistic features and language delay, with or without seizures | 618906 | No |

Abbreviation: HGVS, Human Genome Variation Society; GT, genotype; Het, heterozygote; Hemi, hemizygote; NA, not available; MOI, mode of inheritance; AD, autosomal dominant; AR, autosomal recessive; XD, X-linked dominant; XR, X-linked recessive;

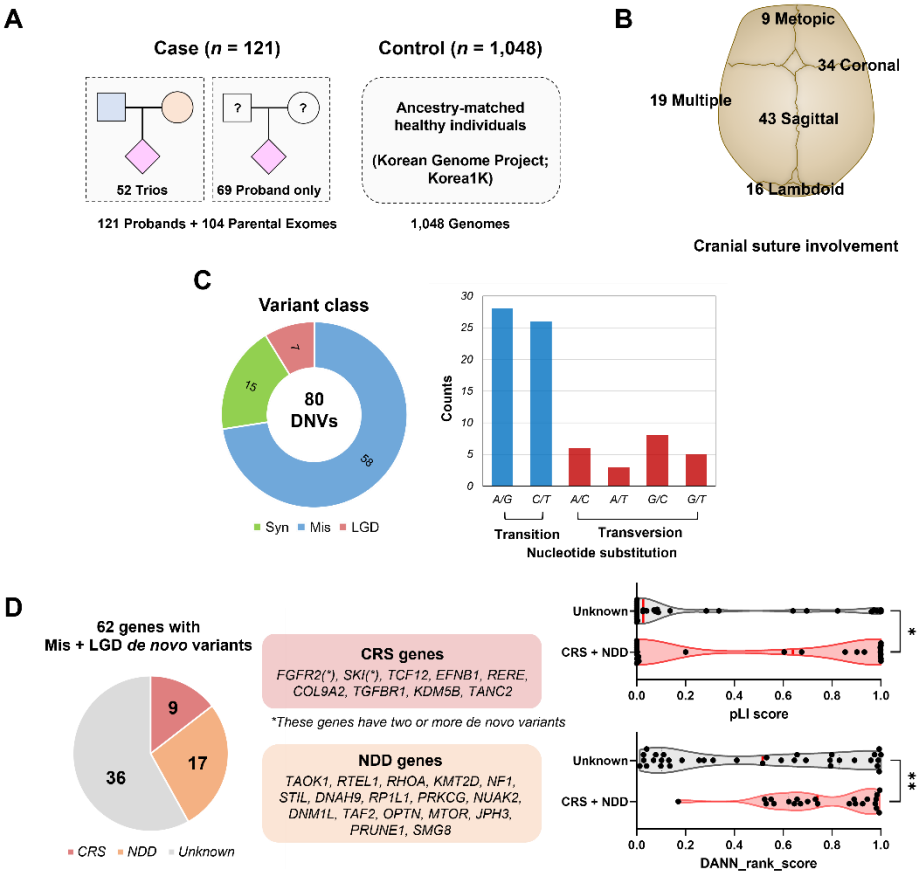


**Figure 1. Study cohort and characterization of *de novo* variants identified in 52 trios.** **(A)** Overview of the craniosynostosis (CRS) cohort and the Korean population control (Korea1K). A total of 121 CRS probands, including 52 trios and 69 proband-only samples, underwent exome sequencing. A population control dataset comprising whole-genome sequencing data from 1,048 unaffected Korean individuals was utilized. **(B)** Distribution and classification of affected cranial sutures in the study cohort. **(C)** Distribution and classification of 80 *de novo* variants identified in the 52 trios. **(D)** Analysis reveals the presence of likely-gene disrupting (LGD) or missense variants in 26 genes associated with CRS or neurodevelopmental disorders (NDD). These genes exhibited a higher degree of haploinsufficiency and deleteriousness, as indicated by higher pLI scores and DANN_rank_score parameters. *$P < 0.05$, ** $P < 0.01$ by Mann-Whitney U test.

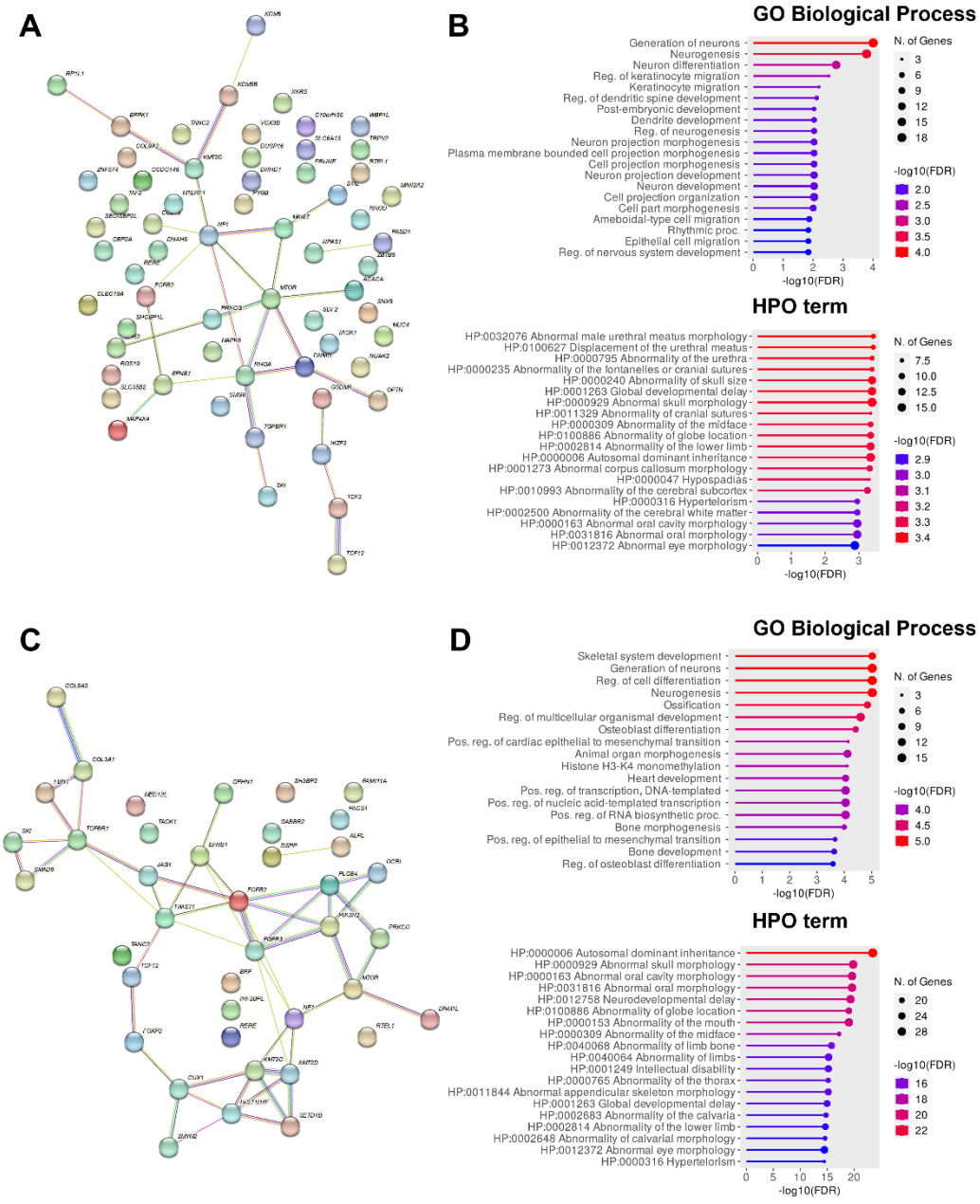


**Figure 2. Gene network and pathway enrichment analyses of genes associated with craniosynostosis.** Gene network and pathway enrichment analyses were conducted on the genes that have functionally altered (likely gene disrupting or missense) *de novo* variants

**(A, B)** or pathogenic (P) or likely pathogenic (LP) variants **(C, D)**. The protein-protein interaction networks of **(A)** the 62 genes with *de novo* variants and **(C)** the 40 genes with P/LP variants show that known craniosynostosis (CRS) genes are frequently located on the cores among many interactions at the molecular level. Pathway enrichment analysis shows that there are significant enrichments of **(B)** the 62 genes with *de novo* variants and **(D)** the 40 genes with P/LP variants in the Gene Ontology (GO) biological processes related to Neurogenesis (GO:0022008) and Ossification (GO:0001503), and human phenotype ontology (HPO) terms related to Abnormality of the fontanelles or cranial sutures (HPO:0000235) and Abnormal skull morphology (HPO:0000929). Our findings suggest that these genes play significant roles in the pathogenesis of CRS.

## 2. Identification of digenic impairments of haploinsufficient genes in CRS patients using exome sequencing

We observed a high proportion of haploinsufficient genes among the known CRS/NDD genes (**Fig 1D**). Also, the well-established dosage effect observed in the *ERF* and *TCF12* genes[6,7] on the CRS phenotype led us to hypothesize that haploinsufficient genes might play a significant role in the development of CRS[33]. Consequently, we conducted exome-wide screening for possible digenic combinations in CRS cases (**Fig. 3A**). We conducted exome-wide screening for possible digenic combinations in CRS cases (**Fig. 3A**). We focused on 2,813 autosomal haploinsufficient genes (pLI > 0.9) and rare functionally deleterious (LGD or deleterious missense [D-mis]) variants. To ensure robust results, we used an exploratory cohort of 52 trios, along with their 104 parents, and a control dataset of 1,048 individuals from the Korean population. We extracted case-specific digenic dominant pairs, excluding combinations observed in parents or population controls. Subsequently, we assessed the pathogenicity of these case-specific pairs using ORVAL[15]. Only digenic pairs classified in the "99.9%-zone disease-causing" category remained (**Fig. 3B,C**). Further investigation was conducted into additional CRS proband-only samples, leading to the identification of six digenic pairs with two independent cases (**Table 5**).

Among the identified genes, all 12 were expressed in the central nervous system, and all variants were D-mis variants. Of these 12 genes, seven were known to be associated with Mendelian disorders in autosomal dominant (AD) or autosomal recessive (AR) inheritance. The genes *TRPS1* (Trichorhinophalangeal syndrome; OMIM: 190350), *CACNA1A* (Developmental and epileptic encephalopathy; OMIM: 617106), *BMP4* (Orofacial cleft; OMIM: 600625), and *TSC2* (Tuberous sclerosis; OMIM:613254) were associated with AD disorders, while *IL6ST* (Stuve-Wiedemann syndrome; OMIM: 619751), *LRP1* (Keratosis pilaris atrophicans; OMIM: 604093), and *COL12A1* (Bethlem myopathy; OMIM: 616471) were associated with AR disorders. With the exception of the cases with the *IL6ST* and *TRPS1* gene pair, the P/LP variants related to CRS (*FGFR2*, *TCF12*, and *ERF*) or NDD (*KMT2D* and *RERE*) genes were also identified either in a trio or proband-only sample of

the other five digenic pairs (**Table 5**), implying that the causative gene combinations would be somewhat complicated in these cases. As a result, we focused on the *IL6ST* and *TRPS1* gene pairs and conducted an *in vitro* study to explore the potential contribution of digenic impairments of these genes to CRS.

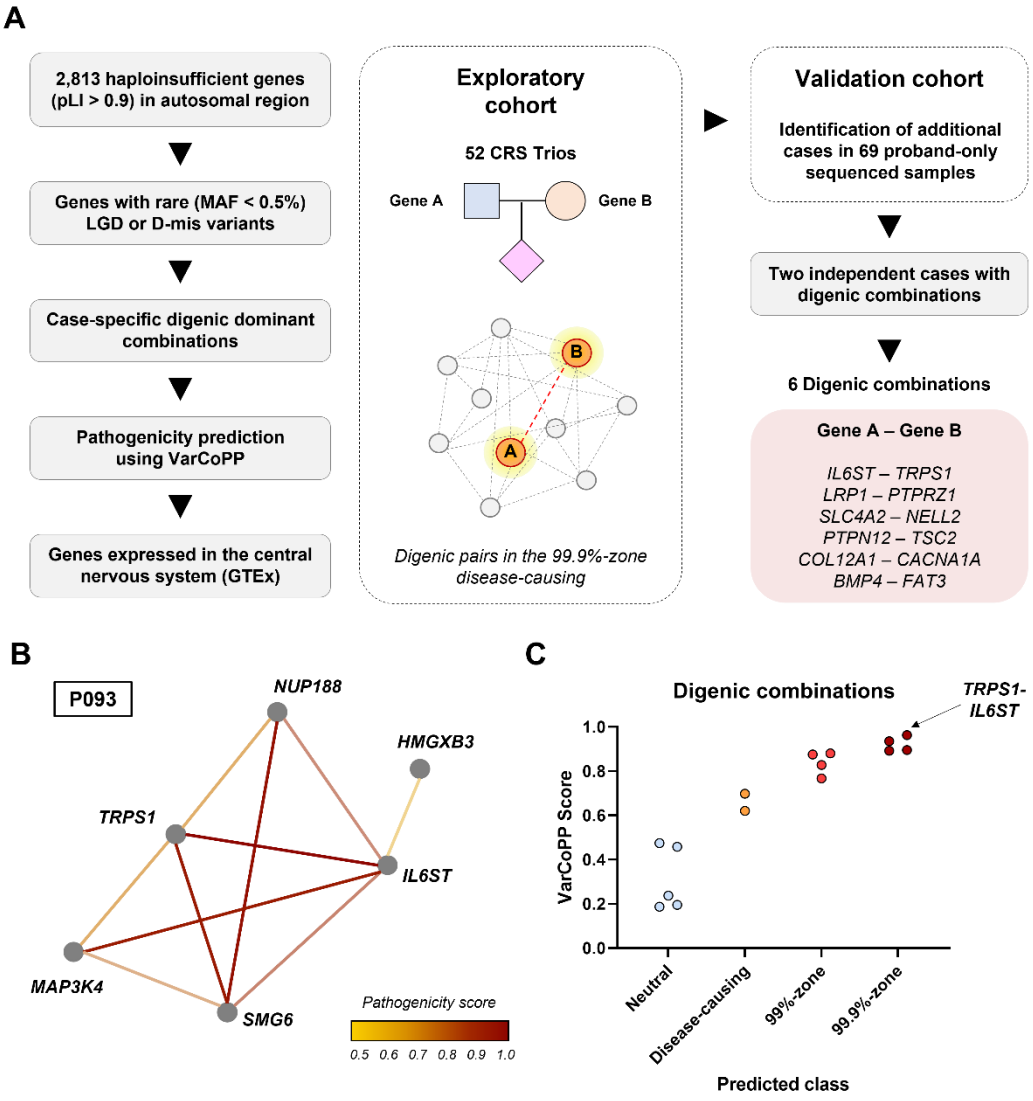


**Figure 3. Identification of digenic combinations in haploinsufficient genes associated with craniosynostosis. (A)** Investigation of rare digenic combinations in haploinsufficient genes (pLI score > 0.9) associated with craniosynostosis. Rare deleterious variants, including likely gene disrupting (LGD) or damaging missense (D-mis) variants, were screened in 52 craniosynostosis (CRS) trios. Digenic combinations observed in unaffected individuals were filtered using unaffected parents and population controls, retaining only

those exclusively present in affected probands. The pathogenicity of case-specific digenic combinations was predicted using VarCoPP. Further analysis focused on digenic pairs falling within the 99.9% confidence zone of disease-causing variants and involved additional sequencing of 69 craniosynostosis probands. Through this approach, six digenic pairs were identified, each observed in two independent cases. **(B)** Illustration of digenic interactions predicted by ORVAL in patient P093. Rare variants were filtered, and their pathogenicity was predicted based on gene-gene interaction networks, following the aforementioned process. **(C)** Prioritization of digenic combinations based on VarCoPP pathogenicity scores classified in the 99.9% zone. The validation cohort of 69 proband-only samples was then evaluated to identify additional cases harboring these digenic combinations.

**Table 5. Case-specific digenic pairs with two unrelated cases identified in this study.**

| Proband | Sex | CRS | Gene A (Transcript) | AA change | Origin | Gene B (Transcript) | AA change | Origin | P/LP variants in CRS or NDD genes |
|---|---|---|---|---|---|---|---|---|---|
| P051 | male | S | *IL6ST* (NM_002184) | p.S248F | NA | *TRPS1* (NM_014112) | p.Q181R | NA | No |
| P093 | female | L | | p.N360S | Pat | | p.R814L | Mat | No |
| P052 | female | C | *LRP1* (NM_002332) | p.R2440W | NA | *PTPRZ1* (NM_002851) | p.F827L | NA | *TCF12* |
| P061 | male | L | | p.S1149L | Pat | | p.E1336G | Mat | No |
| P028 | male | C | *SLC4A2* (NM_003040) | p.R95H | Pat | *NELL2* (NM_001145108) | p.R122W | Mat | *RERE* |
| P132 | female | C | | p.V1155I | NA | | p.A156T | NA | No |
| P032 | female | S | *PTPN12* (NM_002835) | p.S684L | Pat | *TSC2* (NM_000548) | p.K1689R | Mat | No |
| P071 | male | S | | p.L336M | NA | | p.S1383I | NA | *KMT2D* |
| P110 | male | S | *COL12A1* (NM_004370) | p.V1862A | NA | *CACNA1A* (NM_001127222) | p.R2195Q | NA | No |
| P121 | male | S, L | | p.A2760V | Pat | | p.R480C | Mat | *ERF* |
| P049 | female | S | *BMP4* (NM_001202) | p.H251Y | NA | *FAT3* (NM_001367949) | p.Y339C | NA | No |
| P131 | male | C | | p.R162Q | Pat | | p.R433W | Mat | *FGFR2* |

Abbreviation: AA, amino acids; P, pathogenic; LP, likely pathogenic; CRS, cranial suture involvement; S, sagittal; M, metopic; C, coronal; L, lambdoidal; Pat, paternally inherited; Mat, maternally inherited; NA, not available;

**Table 6. Pathogenicity prediction of digenic combinations using the ORVAL.**

| Gene A | Gene B | Gene A alleles | Gene B alleles | VarCoPP score | Predicted class | Confidence zone |
|---|---|---|---|---|---|---|
| ***TRPS1*** | ***IL6ST*** | 8:116599487:C:A | 5:55252041:T:C | 0.9625 | Disease-causing | 99.9%-zone |
| ***NUP188*** | ***IL6ST*** | 9:131765210:G:A | 5:55252041:T:C | 0.935 | Disease-causing | 99.9%-zone |
| ***IL6ST*** | ***SMG6*** | 5:55252041:T:C | 17:1989098:T:G | 0.895 | Disease-causing | 99.9%-zone |
| ***NUP188*** | ***SMG6*** | 9:131765210:G:A | 17:1989098:T:G | 0.8925 | Disease-causing | 99.9%-zone |
| ***TRPS1*** | ***SMG6*** | 8:116599487:C:A | 17:1989098:T:G | 0.88 | Disease-causing | 99.9%-zone |
| ***MAP3K4*** | ***IL6ST*** | 6:161519441:G:A | 5:55252041:T:C | 0.875 | Disease-causing | 99%-zone |
| ***MAP3K4*** | ***SMG6*** | 6:161519441:G:A | 17:1989098:T:G | 0.8275 | Disease-causing | 99%-zone |
| ***MAP3K4*** | ***TRPS1*** | 6:161519441:G:A | 8:116599487:C:A | 0.7675 | Disease-causing | |
| ***NUP188*** | ***TRPS1*** | 9:131765210:G:A | 8:116599487:C:A | 0.6975 | Disease-causing | |
| ***IL6ST*** | ***HMGXB3*** | 5:55252041:T:C | 5:149406325:G:A | 0.62 | Disease-causing | |
| ***SMG6*** | ***HMGXB3*** | 17:1989098:T:G | 5:149406325:G:A | 0.475 | Neutral | |
| ***TRPS1*** | ***HMGXB3*** | 8:116599487:C:A | 5:149406325:G:A | 0.4575 | Neutral | |
| ***NUP188*** | ***HMGXB3*** | 9:131765210:G:A | 5:149406325:G:A | 0.2375 | Neutral | |
| ***MAP3K4*** | ***HMGXB3*** | 6:161519441:G:A | 5:149406325:G:A | 0.195 | Neutral | |
| ***MAP3K4*** | ***NUP188*** | 6:161519441:G:A | 9:131765210:G:A | 0.1875 | Neutral | |

This table provides the pathogenicity predictions for digenic combinations using ORVAL in proband P093. Rare variants were filtered according to the method described in Figure 2, and the pathogenicity of each digenic combination was predicted individually. ORVAL utilizes gene-gene interaction networks and the pathogenicity of each variant combination to predict the pathogenicity of digenic combinations. Digenic combinations with disease-causing potential, exhibiting segregated alleles in the 99.9% zone, were further evaluated in the validation cohort to identify additional cases harboring these combination.

## 3. Digenic impairments of IL6ST and TRPS1 in non-syndromic CRS

We identified two patients (P051 and P093; **Fig. 4,5**) with non-syndromic CRS who carried D-mis variants in the *IL6ST* and *TRPS1* genes (**Fig. 4A**). These variants were found at highly conserved sites across mammalian species (**Fig. 4B**). The affected cranial sutures were the sagittal and right lambdoidal lines in the patients P051 and P093, respectively (**Fig. 4C,D**). Structural predictions indicated that the N360S and S580F variants in the *IL6ST* gene (encoding GP130) were situated in the fibronectin type III domains of extracellular regions with high confidence prediction (**Fig. 4E**). In contrast, the *TRPS1* Q181R and R814L variants were located in unstructured regions (**Fig. 4F**).

Given the involvement of *IL6ST* and *TRPS1* in bone ossification[19] and the previously reported association of *IL6ST* with CRS in a biallelic AR pattern[34], we further evaluated the functional effects of the identified *IL6ST* and *TRPS1* variants. The IL6ST functional activity was analyzed using the IL6 sis-inducible element (SIE/STAT3) dual-luciferase reporter assay upon IL-11 stimulation with the exogenous expression of wild-type and variant IL6ST proteins in HEK293 cells (**Fig. 7C**). The cells were pretreated with a siRNA against the 3'-untranslated region (UTR) of *IL6ST* to eliminate confounding effects incurred from the endogenous IL6ST (**Fig. 7A**). The IL6ST activity measurements using the reporter assays revealed that the IL6ST N360S and S580F variants exhibited decreased activity, with WT levels of 65% and 48%, respectively (**Fig. 7C**). Control immunoblot analyses showed that the IL6ST mutations did not affect protein expression levels (**Fig. 7E**).

TRPS1 is an inhibitory regulator of osteocalcin transcription and osteogenic differentiation, and acts as a transcriptional repressor in the osteoblast-specific *cis*-acting element (OSE2) reporter assay[19]. HepG2 cells that minimally express endogenous TRPS1 were employed to avoid potential effects from the endogenous TRPS1 expression (**Fig. 7B**). The repressor activity of TRPS1 against the RUNX2-mediated OSE2 transcriptional activation was measured using the dual-luciferase reporter assay (**Fig. 7D**). Notably, the TRPS1 Q181R and R814L variants displayed a reduced repressor activity on the OSE2

reporter activation, with WT levels of 60% and 26.7%, respectively (**Fig. 7D**). Immunoblot analyses revealed that protein expression levels were not altered by the TRPS1 mutations (**Fig. 7E**).

Although *TRPS1* is known to be associated with Trichorhinophalangeal syndrome (OMIM: 190350) in an AD inheritance pattern, the maternal inheritance of the same *TRPS1* R814L variant, along with none of its clinical features observed in patient P093, indicate that CRS in this case is not attributable to Trichorhinophalangeal syndrome (**Fig. 4C**). Collectively, our experimental findings indicate that the *IL6ST* and *TRPS1* variants identified in this study are hypomorphs, resulting in reduced protein activity; however, each gene variant is not pathogenic in isolation.

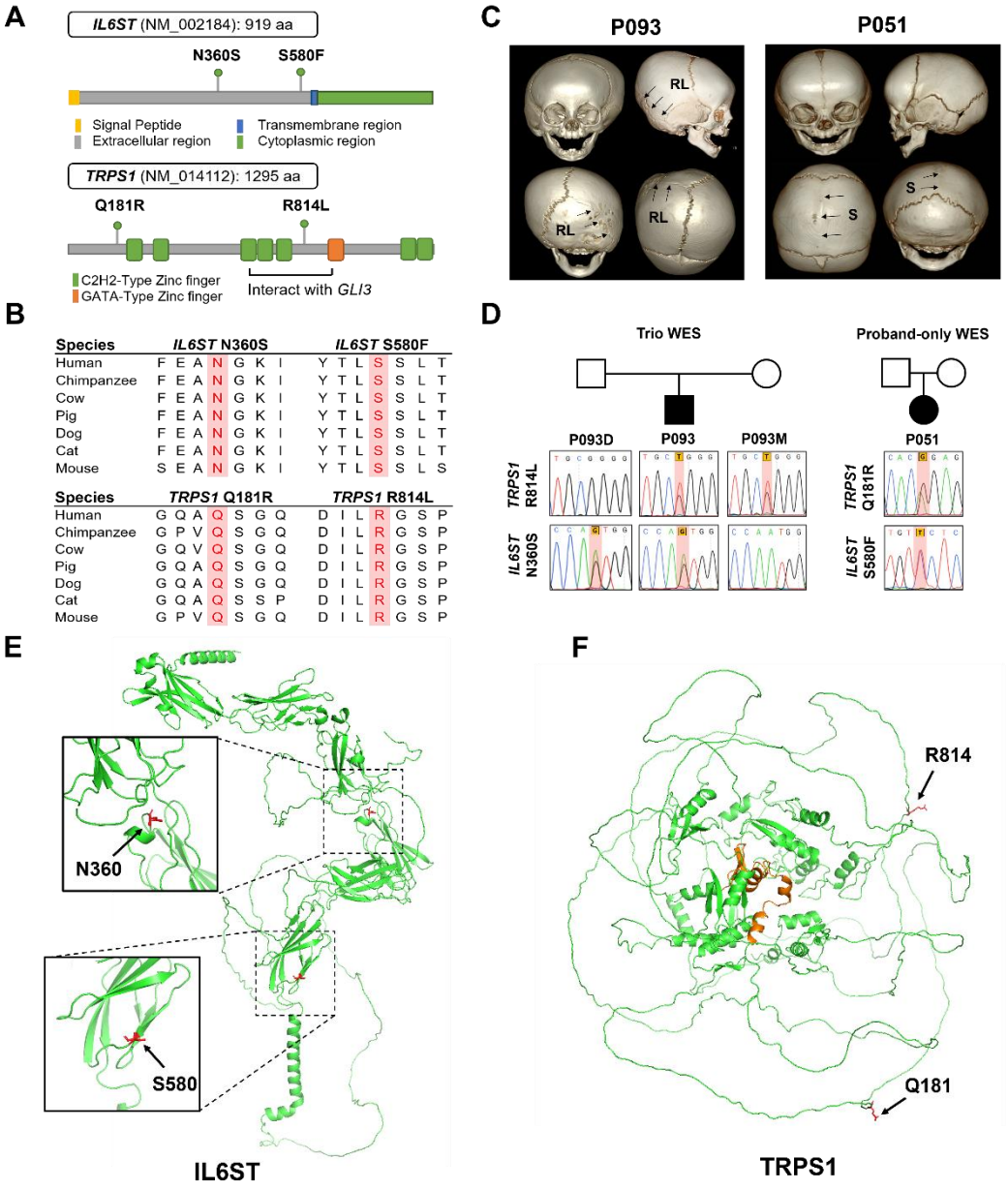


**Figure 4. Characterization of craniosynostosis patients with digenic impairments in *TRPS1* and *IL6ST*. (A, B)** Schematic representation of the variants identified in the *TRPS1* and *IL6ST* genes. The positions of all variants are indicated, and they are shown to be

located in highly conserved sites across mammalian species. **(C, D)** Pedigree and genotype information of the non-syndromic craniosynostosis patients (P093 and P051). The 3D reconstruction images of skull computed tomography reveal premature fusions of lambdoidal and sagittal sutures (indicated by black arrows) in patients P093 and P051, respectively **(E)** The transmembrane protein GP130, encoded by IL6ST, is depicted with two variants (N360S and S580F) located in extracellular domains. These variants exhibited reduced activities compared to the wild-type. **(F)** TRPS1, a nuclear transcription factor, was partially predicted by AlphaFold. The core structures, including the GATA-type Zn finger domain highlighted in orange, were well-predicted. The two variants (Q181R and R814L) were found outside the GATA-type Zn finger domain, which is associated with trichorhinophalangeal syndrome. These variants showed lower transcriptional repression activities than the wild-type.

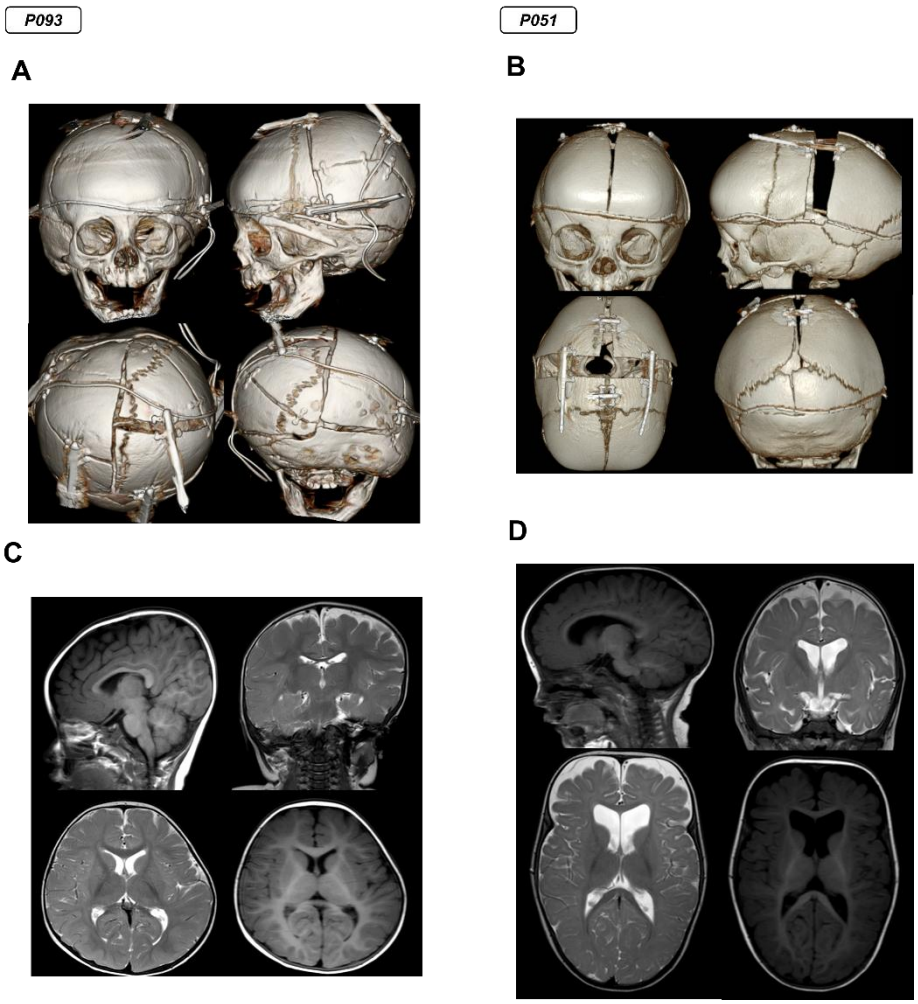


**Figure 5. Clinical information of patients with TRPS1 and IL6ST variants.** The figure depicts clinical data of two craniosynostosis patients (P051, P093) with no family history of the condition. Skull deformity was identified after 4-6 months of birth, leading to diagnosis through Skull X-ray and CT imaging. Distraction osteogenesis was performed within the first year of birth (P051: 6 months, P093: 11 months) without any complications. Post-surgery CT **(A, B)** and MRI images **(C, D)** showed successful correction and normal brain structure, and continuous follow-up indicated average development in both patients.

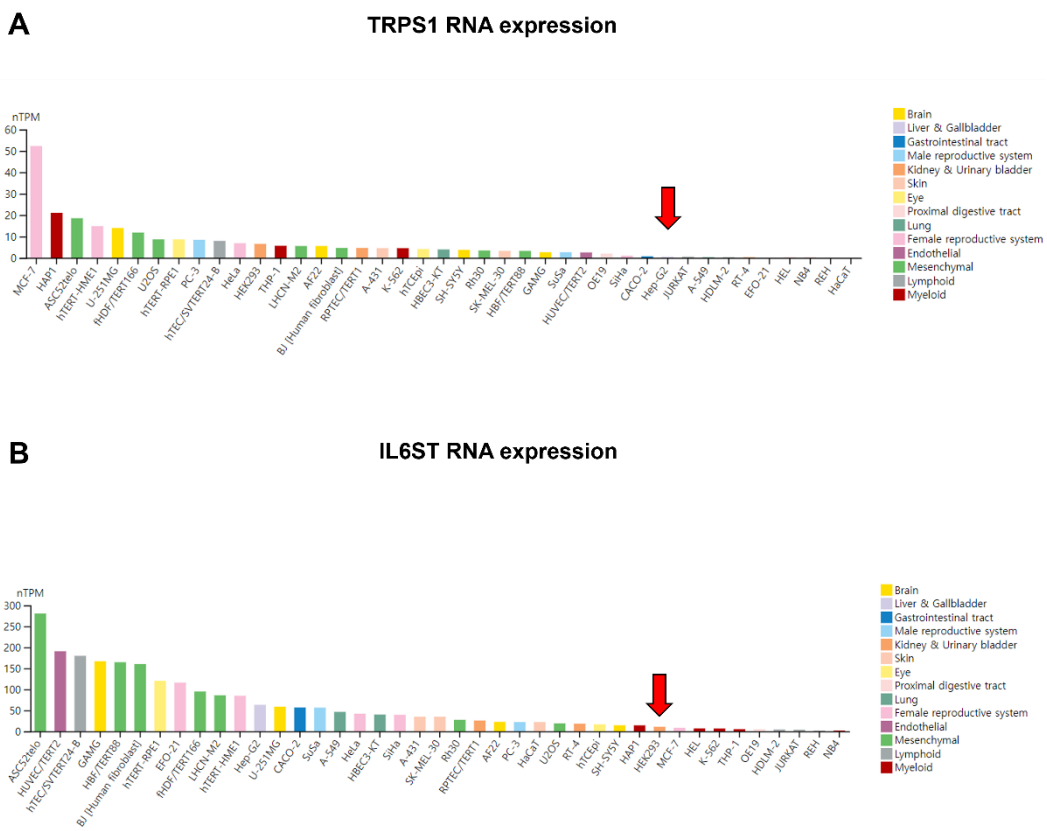


**Figure 6. Expression levels of TRPS1 and IL6ST in different cell lines for assessment of variant activities. (A)** Expression levels of IL6ST across various tissues based on GTEx data. Due to the widespread expression of IL6ST, HEK293 cells were chosen, and endogenous expression was downregulated using siRNA. **(B)** Expression levels of TRPS1 across various tissues based on GTEx data. Liver tissues (red arrow) exhibited the lowest TRPS1 expression levels, prompting the selection of HepG2 cells for the evaluation of TRPS1 mutant activity.

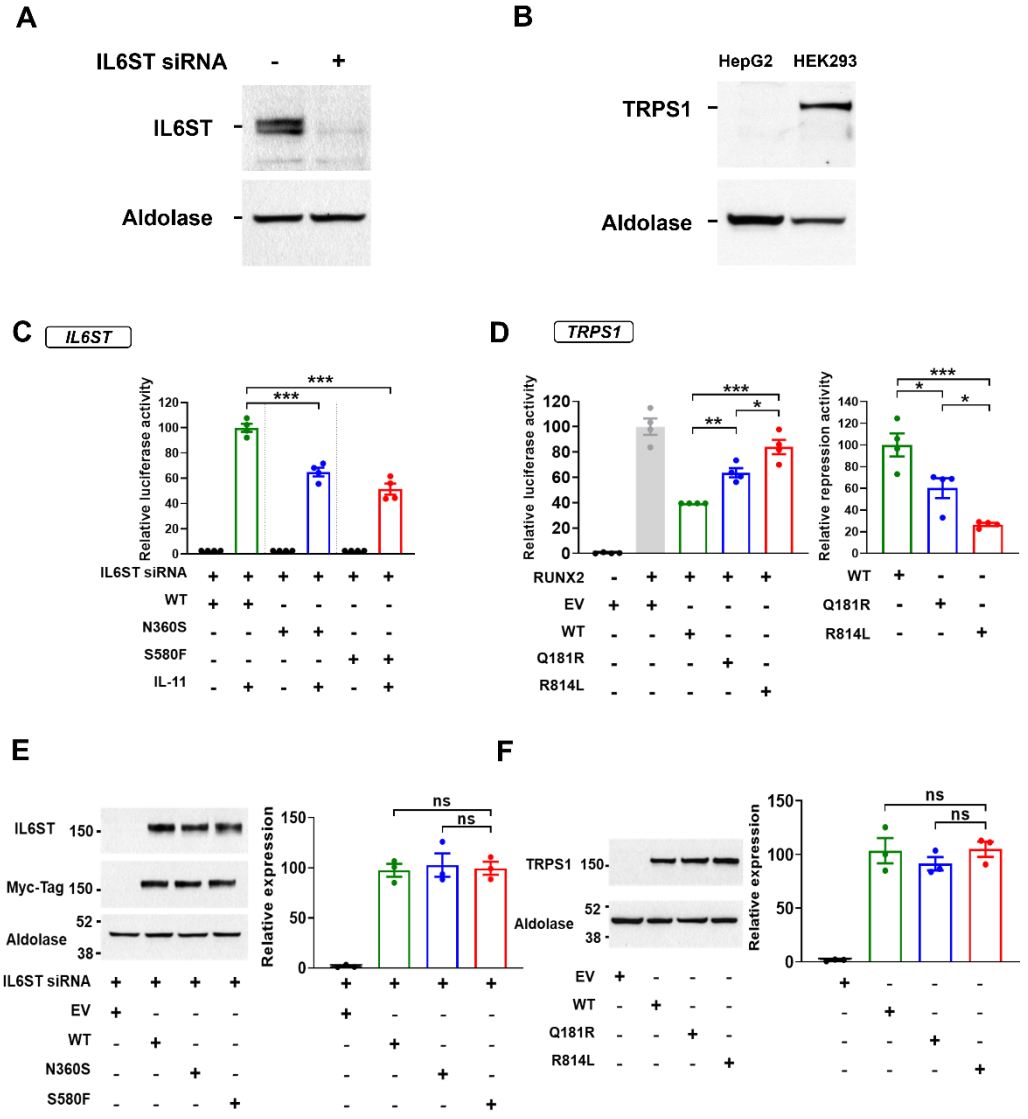


**Figure 7. Functional analysis of variants of TRPS1 and IL6ST. (A)** Knockdown of endogenous IL6ST expression in HEK293 cells using siRNA against the 3'-untranslated region of IL6ST. Western blot results demonstrate efficient suppression of IL6ST expression via siRNA treatment. **(B)** Western blot analysis of TRPS1 protein levels in HepG2 and HEK293 cell lines. The results confirm the absence of endogenous TRPS1

expression in HepG2 cells. **(C)** The IL6ST functional activity was measured using the IL6 sis-inducible element (SIE/STAT3) dual-luciferase reporter assays with IL-11 stimulation in HEK293 cells. To eliminate the potential effects of endogenous IL6ST, cells were treated with siRNA against the 3'-UTR of IL6ST 6 h before plasmid transfection. Cells were then transfected with plasmids for 1) dual luciferase assay (pGL4.47 [luc2P/SIE/Hygro] and pGL4.70 [hRluc]), 2) IL11 receptor, and 3) wild-type or variant IL6ST. The SIE/STAT3 transcriptional activities were measured with human IL-11 (1 ng/ml) stimulation for 6 h. The N360S and S580F variants showed lower IL6ST functional activity than wild-type (WT). **(E)** Immunoblot analyses showing comparable protein expression levels among WT and variant IL6STs. **(D)** The TRPS1 functional activity was measured using the osteoblast-specific *cis*-acting element (OSE2) reporter assay in HepG2 cells that minimally express endogenous TRPS1 (**Fig. 6)**. Cells were co-transfected with plasmids for RUNX2 to activate the OSE2 reporter transcriptional activity. Subsequently, the TRPS1-mediated transcriptional repression activity was measured using the dual luciferase assay in cells transfected with wild-type or variant TRPS1 plasmids. The Q181R and R814L variants showed lower TRPS1 activity than WT. **(F)** Immunoblot analyses showing comparable protein expression levels among WT and TRPS1 variants. n.s.: not significant. $*P < 0.05$, $**P < 0.01$, $***P < 0.001$ by one-way ANOVA followed by Tukey's multiple comparison test.

## 4. Accelerated bone mineralization in osteoblasts induced by IL6ST and TRPS1 downregulation

To investigate the effects of *IL6ST* and *TRPS1* hypomorphic mutants on intramembranous ossification, simultaneous knockdowns of *IL6ST* and *TRPS1* were conducted in the MC3T3E1 murine calvaria cells using combinations of gene-specific siRNAs (**Fig. 8A**). The knockdown efficiency of each gene was measured via qRT-PCR analysis 48 h after the siRNA transfection. As shown in **Fig. 8B**, a 50-70% reduction in mRNA levels in the target gene was achieved via transfections with appropriate concentrations of each siRNA. Combinations of both siRNAs did not greatly affect the mRNA levels of each gene, indicating no significant interference between the siRNAs used (**Fig. 8B**). Analyses of alkaline phosphatase (ALP) staining results revealed that knockdowns of *IL6ST* resulted in no significant change, whereas *TRPS1* exerted a partial increase in bone mineralization. Notably, the dual knockdown of *IL6ST* and *TRPS1* resulted in a synergistic effect showing the highest level of bone mineralization (**Fig. 8C**). The synergistic effect of *IL6ST* and *TRPS1* double knockdown was further confirmed via the ALP activity assay (**Fig. 8D**). Furthermore, mRNA expression levels of genes associated with osteogenic differentiation, including ALPL, BGLAP, IBSP, COL1A1, and RUNX2, all showed an additive or potentiation effect of *IL6ST* and *TRPS1* double gene knockdown on osteoblastogenesis in the MC3T3E1 cells (**Fig. 8E**). In an immunoblot assay identifying the signaling pathways responsible for bone mineralization, the phosphorylated forms of AKT were prominently reduced in the cells with the double gene knockdown (**Fig. 8E**). In aggregate, these results imply that simultaneous reductions in IL6ST and TRPS1 activity can accelerate bone mineralization, potentially contributing to the development of CRS.

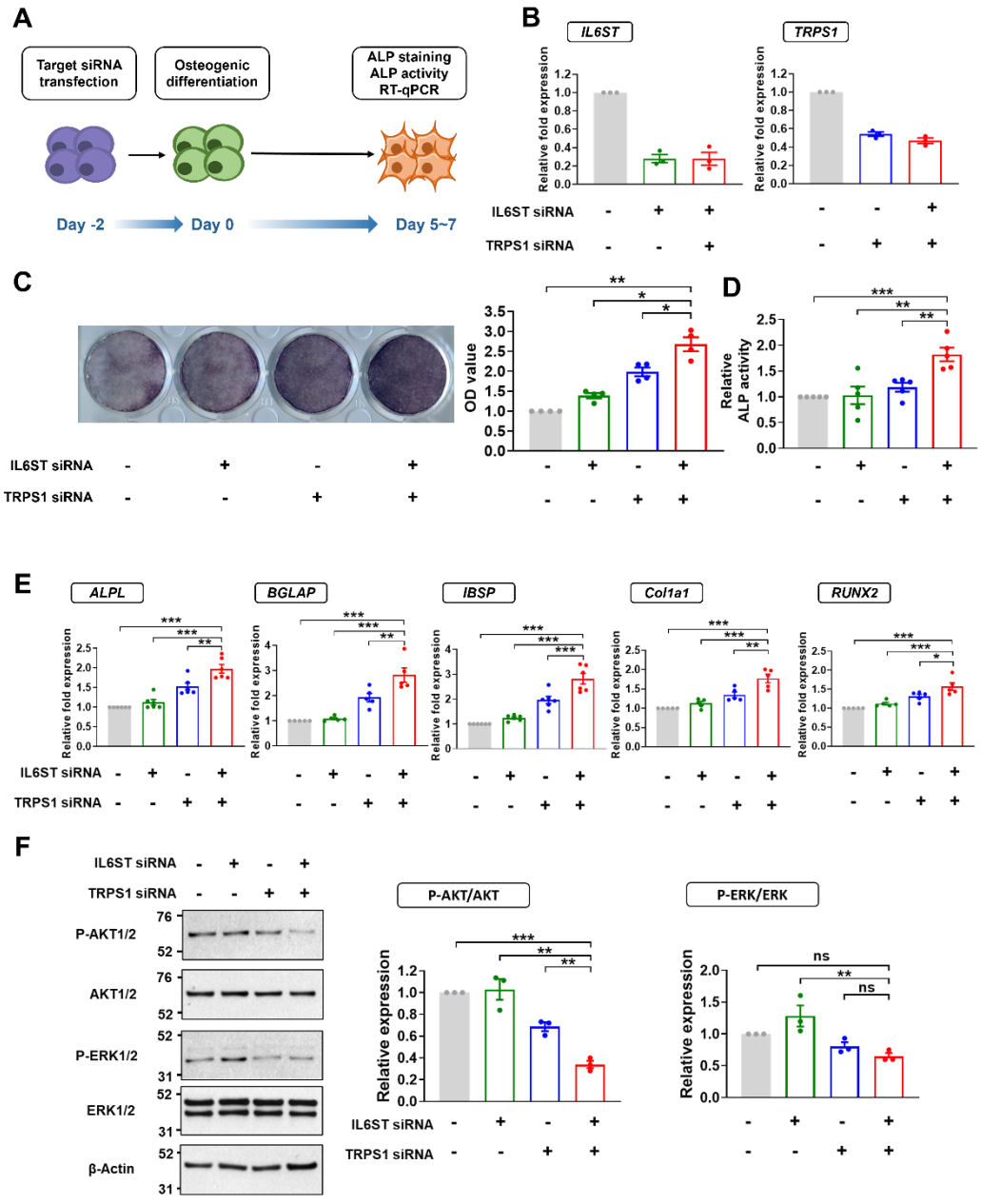


**Figure 8. Additive effects of TRPS1 and IL6ST double knockdown on bone mineralization in osteoblast. (A)** Schematic presentation of osteoblast differentiation

process in mouse calvarial cells (MC3T3E1). Treatment with IL6ST and TRPS1 siRNA was performed 48 h before induction of differentiation. Osteogenic medium was replenished every 3 days, and the differentiation was evaluated on day 5 ~ 7 after osteogenic induction. **(B)** Measurement of IL6ST and TRPS1 expression levels using qRT-PCR after 48 h of siRNA transfection (IL6ST: 25 nM, TRPS1: 25 nM) using Lipofectamine RNAiMAX ($n$ = 3, biologically independent samples). **(C, D)** ALP staining and measurement of ALP activity conducted on day 5 after induction of differentiation. The double siRNA treated groups exhibited the most prominent ALP activity, indicating the highest osteoblast differentiation. **(E)** Measurement of osteogenic markers (ALPL, BGLAP, IBSP, COL1A1, and RUNX2) by qRT-PCR on day 5 after osteogenic induction. ($n$ = 5 or 6, biologically independent samples). **(F)** Representative Western blot images depicting the protein expression levels of phosphorylated AKT1/2 (P-AKT1/2), and phosphorylated ERK1/2 (P-ERK1/2) in the MC3T3E1 cell line after 6 h of differentiation period. Densitometry-based quantification of the Western blot results, presenting relative protein expression levels as mean ± s.d. ($n$ = 3, biological replicates). Remarkably, double knockdown groups treated with IL6ST and TRPS1 siRNA exhibited synergistic effects on phospho-AKT levels, consistent with the observed trends in osteogenic markers. Statistical significance was determined using ordinary one-way ANOVA with Tukey's test for multiple comparisons. n.s.: not significant. *$P$ < 0.05, **$P$ < 0.01, ***$P$ < 0.001 by one-way ANOVA followed by Tukey's multiple comparison test.

## 5. No additive effects of IL6ST and TRPS1 down regulation on osteoclast differentiation

Considering that bone homeostasis is achieved via a balanced regulation of osteoblasts and osteoclasts, we also assessed the impact of *TRPS1* and *IL6ST* downregulation on osteoclastogenesis using the osteoclast-derived RAW 264.7 cells (**Fig. 9A**). The knockdown efficiency determined by qRT-PCR analyses (48 h after siRNA transfection) showed that a 50-60% reduction in TRPS1 and IL6ST mRNA expression was achieved via treatment with appropriate concentrations of gene-specific RNAs in RAW264.7 cells (**Fig. 9B**). To assess the osteoclastogenesis and osteoclast differentiation, the presence of differentiated multinucleated giant cells was analyzed using tartrate-resistant acid phosphatase (TRAP) staining. Interestingly, treatments with siRNAs against *TRPS1* displayed a reduced osteoclast differentiation, while those against *IL6ST* did not exhibit discernible changes. Furthermore, no additive effects were observed in cells treated with combinations of both siRNAs (**Fig. 9C,D and Fig 10**). Similar findings were also identified in the quantification of the mRNA expression levels of osteoclast marker genes, such as CTSK, DCSTAMP, TRAP, and NFATc1 (**Fig. 9E**). Collectively, these results suggest that the downregulation of TRPS1 alone hinders osteoclastogenesis, while there are no additional effects when IL6ST is simultaneously reduced.

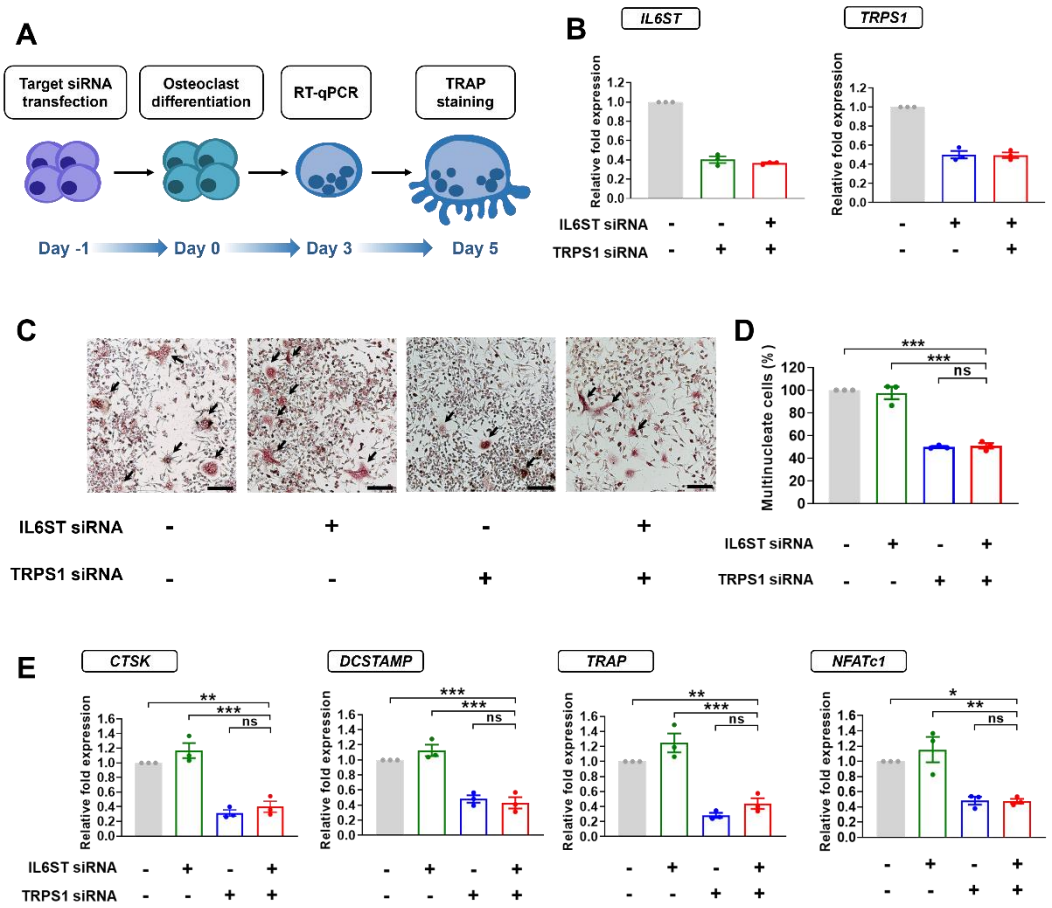


**Figure 9. Combined knockdown of TRPS1 and IL6ST does not show additive effect on osteoclastogenesis. (A)** Schematic depiction of the osteoclast differentiation process in mouse macrophage cells (RAW264.7 cells). RAW264.7 cells were cultured and transfected with siRNA 24 h prior to differentiation, which was induced by the addition of RANKL; and qRT-PCR and TRAP staining were performed on day 3 and day 5, respectively. **(B)** Measurement of IL6ST and TRPS1 expression levels using qRT-PCR after 48 h of siRNA transfection (IL6ST: 12.5 nM, TRPS1: 25 nM) using TransIT-LT1 Transfection Reagent (*n* = 3, biologically independent samples). **(C, D)** Representative images of TRAP staining on day 5 after initiation of differentiation (Scale bar = 100 μm). The cell count of osteoclasts (indicated by black arrows; multi-nucleated cells) was normalized to 100% based on the

scrambled group. **(E)** Expression analysis of osteoclast differentiation marker genes (CTSK, DCSTAMP, TRAP, and NFATc1) using qRT-PCR on day 3 ($n = 3$, biologically independent samples). The expression levels of osteoclast differentiation markers further confirm that the combined knockdown of TRPS1 and IL6ST does not induce an additive effect on osteoclastogenesis. n.s.: not significant. *$P < 0.05$, **$P < 0.01$, ***$P < 0.001$ by one-way ANOVA followed by Tukey's multiple comparison test.

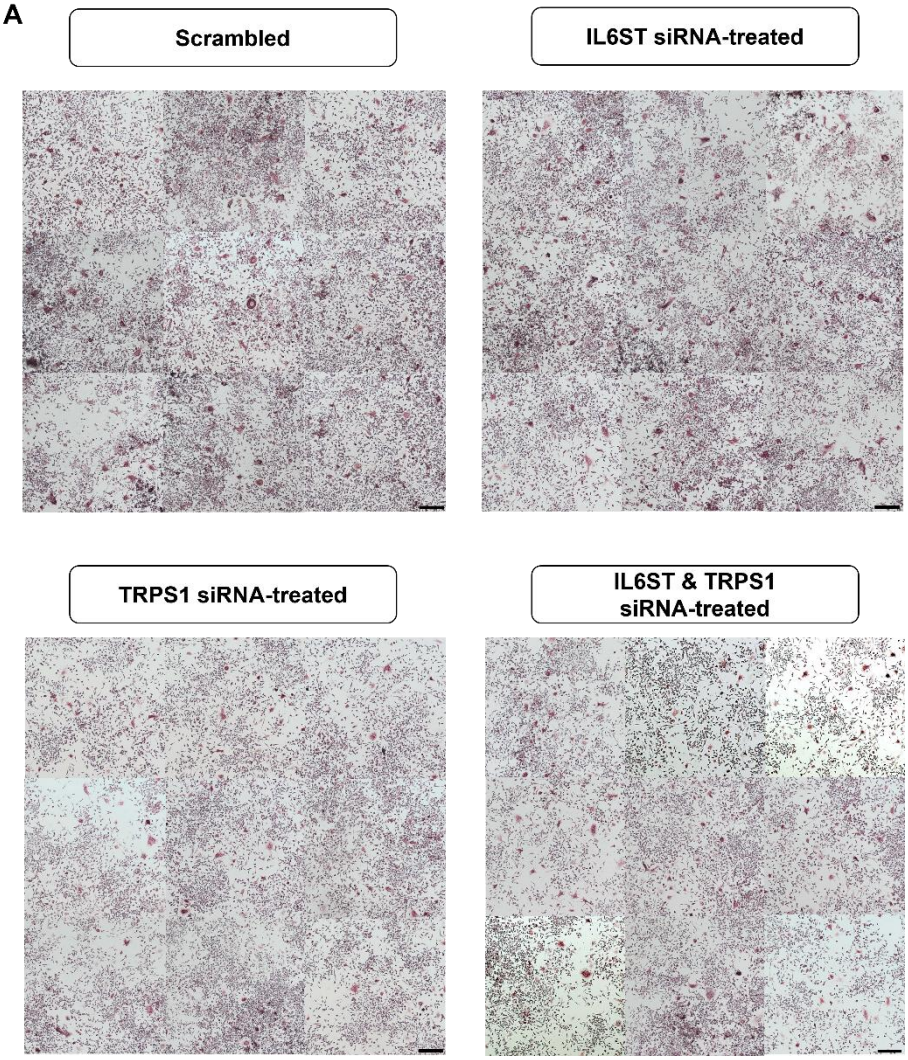


**Figure 10. Representative images of tartrate-resistant acid phosphatase (TRAP) staining to assess osteoclast differentiation.** TRAP staining was performed on day 5 after initiation of differentiation to evaluate osteoclast formation. Images were captured at 9 different locations per well and subsequently combined. The quantification of multi-nucleated cells was conducted on biologically independent samples ($n$ = 3). The scale bar represents 100 μm.

# 4. DISCUSSION

Our understanding of the molecular underpinnings of CRS remains limited, particularly in non-syndromic cases where diagnostic success rates have been lower than those in syndromic cases[1]. Despite the identification of over 100 genes linked to CRS, their clinical interpretation for molecular diagnosis has been challenging due to factors such as incomplete penetrance and weak associations[2,3]. To address these knowledge gaps, our study aimed to investigate the genetic architecture of CRS by utilizing WES in a cohort of 121 CRS probands. Specifically, we explored the potential role of digenic models involving haploinsufficient genes.

Our findings underscore the significance of rare variant burdens in haploinsufficient genes as major genetic drivers of CRS. By focusing on digenic combinations of haploinsufficient genes, we were able to capture pathogenic mechanisms that may be overlooked in a monogenic framework.

We identified six specific digenic gene pairs that were repetitively associated with CRS, and these pairs exhibited highly deleterious *in silico* predictions. Among these gene pairs, we focused on the *TRPS1* and *IL6ST* pair, which was observed in two independent cases of non-syndromic CRS without any further pathogenic variants associated with CRS or NDDs (**Table 4**). We then evaluated the combined effects of these gene variants on the pathogenic mechanisms of CRS. Notably, the present experimental results indicate that simultaneous *TRPS1* and *IL6ST* impairments lead to accelerated bone mineralization in the MC3T3E1 calvaria osteoblast cells, closely resembling CRS development. This suggests that the interaction between these two genes may play a role in cranial suture development and contribute to the pathogenesis of CRS.

The role of *TRPS1* as a repressor of bone formation and its association with bone ossification are well-established. Previous studies have demonstrated that knockdown of TRPS1 leads to accelerated osteoblast differentiation[19]. Our *TRPS1* variants are not located in the mutation hotspots causing the Trichorhinophalangeal syndrome, such as the GATA-type Zn finger domain (894-952 residues, **Fig. 4A**). The results from the OSE2 reporter

assay indicate that the TRPS1 Q181L and R814L variants are hypomorphs in terms of inhibiting the RUNX2-mediated transcriptional activation. The R814L variant has a higher loss-of-function effect compared to the Q181L variant, with a decrease of 73% versus 40% (**Fig. 7D**). The more reduced activity of the R814L variant may be attributed to its location being close to the domains known to interact with *GLI3,* which play an important role in the downstream signaling of TRPS1 (**Fig. 4A**)[35]. *GLI3* is recognized as a repressor of osteoblast function, and loss-of-function mutations in *GLI3* have been linked to CRS in mouse models[36].

The GP130 cytokine receptor subunit encoded by *IL6ST* is the shared receptor for the interleukin (IL)-6 cytokine family, including the IL-6, IL-11, IL-27, leukemia inhibitory factor (LIF), oncostatin M (OSM), ciliary neurotrophic factor (CNTF), cardiotrophin 1 (CT1), and cardiotrophin-like cytokine (CLC). It has been reported that some biallelic loss-of-function mutations in the *IL6ST* gene are associated with CRS [37,38], while the GP130-mediated signaling in general is known to be required for normal osteoblastic function. The *IL6ST* N360S and S580F variants identified in our patients exhibited low SIE/STAT3-mediated transcriptional activity upon IL11 stimulation (**Fig. 7C**). Interestingly, the partial gene knockdown of *IL6ST* has no effect on osteogenic differentiation, while it showed additive/potentiation effects when combined with *TRPS1* partial knockdown in the MC3T3E1 calvaria cells (**Fig. 8C-E**). Given that the GP130 (IL6ST) complex transduces signals from multiple cytokine families at the cell membrane and is responsible for various phenotypes via the stimulation and inhibition of multiple signaling pathways, the precise mechanism of IL6ST knockdown appears to be complicated and has yet to be resolved. A potential mechanism would be the upstream and downstream signaling cascades related to AKT activation, of which phosphorylation highly correlates with the osteogenic differentiation induced by the *TRPS1* and *IL6ST* gene knockdowns (**Fig. 8F**). Previous studies have demonstrated that the inactivation of AKT1 promotes osteoblast differentiation, while reducing osteoclast resorption[39]. These findings are consistent with our results and support the potential role of AKT signaling in the development of CRS.

Being different from the effects in the MC3T3E1 osteoblasts, only *TRPS1* downregulation affected osteoclastogenesis and the double *TRPS1* and *IL6ST* gene knockdown showed no additive effects in the RAW 264.7 osteoclast cells (**Fig. 9,10**), suggesting that accelerated osteogenesis could be primarily responsible for the *TRPS1* and *IL6ST* variants-induced CRS. However, considering that balanced osteoblast and osteoclast activities determine bone homeostasis, the reduced osteoclastogenesis evoked by *TRPS1* hypomorphs may also contribute to the CRS phenotype presentation in patients with these variants.

# 5. CONCLUSION

In the present study, we have shown that CRS patients have a high burden of deleterious missense variants in haploinsufficient genes, and that interactions among genes carrying rare variants could contribute to the non-syndromic CRS phenotype. These results highlight the significant role of rare variants in haploinsufficient genes and expand the genetic spectrum of CRS to digenic or oligogenic inheritances. Future studies with larger cohorts may yield further evidence for the oligogenic architecture of CRS and the biological consequences of gene-gene interactions in cranial suture biology.

# REFERENCES

1 Wilkie, A. O. M., Johnson, D. & Wall, S. A. Clinical genetics of craniosynostosis. *Curr Opin Pediatr* **29**, 622-628 (2017).
2 Twigg, S. R. & Wilkie, A. O. A Genetic-Pathophysiological Framework for Craniosynostosis. *Am J Hum Genet* **97**, 359-377 (2015).
3 Goos, J. A. C. & Mathijssen, I. M. J. Genetic Causes of Craniosynostosis: An Update. *Mol Syndromol* **10**, 6-23 (2019).
4 Timberlake, A. T. *et al.* De novo mutations in inhibitors of Wnt, BMP, and Ras/ERK signaling pathways in non-syndromic midline craniosynostosis. *Proc Natl Acad Sci U S A* **114**, E7341-E7347 (2017).
5 Yoon, J. G. *et al.* Molecular Diagnosis of Craniosynostosis Using Targeted Next-Generation Sequencing. *Neurosurgery* **87**, 294-302 (2020).
6 Twigg, S. R. *et al.* Reduced dosage of ERF causes complex craniosynostosis in humans and mice and links ERK1/2 signaling to regulation of osteogenesis. *Nat Genet* **45**, 308-313 (2013).
7 Sharma, V. P. *et al.* Mutations in TCF12, encoding a basic helix-loop-helix partner of TWIST1, are a frequent cause of coronal craniosynostosis. *Nat Genet* **45**, 304-307 (2013).
8 Lupski, J. R., Belmont, J. W., Boerwinkle, E. & Gibbs, R. A. Clan genomics and the complex architecture of human disease. *Cell* **147**, 32-43 (2011).
9 Gifford, C. A. *et al.* Oligogenic inheritance of a human heart disease involving a genetic modifier. *Science* **364**, 865-870 (2019).
10 Kim, A. *et al.* Integrated clinical and omics approach to rare diseases: novel genes and oligogenic inheritance in holoprosencephaly. *Brain* **142**, 35-49 (2019).
11 Duerinckx, S. *et al.* Digenic inheritance of human primary microcephaly delineates centrosomal and non-centrosomal pathways. *Hum Mutat* **41**, 512-524 (2020).
12 Timberlake, A. T. *et al.* Two locus inheritance of non-syndromic midline craniosynostosis via rare SMAD6 and common BMP2 alleles. *Elife* **5** (2016).
13 Calpena, E. *et al.* SMAD6 variants in craniosynostosis: genotype and phenotype evaluation. *Genet Med* **22**, 1498-1506 (2020).
14 Gustafson, J. A., Park, S. S. & Cunningham, M. L. Calvarial osteoblast gene expression in patients with craniosynostosis leads to novel polygenic mouse model. *PLOS ONE* **14**, e0221402 (2019).
15 Renaux, A. *et al.* ORVAL: a novel platform for the prediction and exploration of disease-causing oligogenic variant combinations. *Nucleic Acids Res* **47**, W93-W98 (2019).
16 Pounraja, V. K. & Girirajan, S. A general framework for identifying oligogenic combinations of rare variants in complex disorders. *Genome Res* **32**, 904-915 (2022).
17 Karczewski, K. J. *et al.* The mutational constraint spectrum quantified from variation in 141,456 humans. *Nature* **581**, 434-443 (2020).
18 Satterstrom, F. K. *et al.* Large-Scale Exome Sequencing Study Implicates Both Developmental and Functional Changes in the Neurobiology of Autism. *Cell* **180**, 568-584 e523 (2020).
19 Piscopo, D. M., Johansen, E. B. & Derynck, R. Identification of the GATA factor TRPS1 as a repressor of the osteocalcin promoter. *J Biol Chem* **284**, 31690-31703 (2009).
20 Jeon, S. *et al.* Korean Genome Project: 1094 Korean personal genomes with clinical information. *Sci Adv* **6**, eaaz7835 (2020).
21 Liu, X., Li, C., Mou, C., Dong, Y. & Tu, Y. dbNSFP v4: a comprehensive database of

transcript-specific functional predictions and annotations for human nonsynonymous and splice-site SNVs. *Genome Med* **12**, 103 (2020).

22 Karczewski, K. J. *et al.* The mutational constraint spectrum quantified from variation in 141,456 humans. *Nature* **581**, 434-443 (2020).

23 Amberger, J. S., Bocchini, C. A., Scott, A. F. & Hamosh, A. OMIM.org: leveraging knowledge across phenotype–gene relationships. *Nucleic Acids Res* **47**, D1038-D1043 (2018).

24 Li, Q. & Wang, K. InterVar: Clinical Interpretation of Genetic Variants by the 2015 ACMG-AMP Guidelines. *Am J Hum Genet* **100**, 267-280 (2017).

25 Jian, X., Boerwinkle, E. & Liu, X. In silico prediction of splice-altering single nucleotide variants in the human genome. *Nucleic Acids Res* **42**, 13534-13544 (2014).

26 Quang, D., Chen, Y. & Xie, X. DANN: a deep learning approach for annotating the pathogenicity of genetic variants. *Bioinformatics* **31**, 761-763 (2015).

27 Poplin, R. *et al.* A universal SNP and small-indel variant caller using deep neural networks. *Nat Biotechnol* **36**, 983-987 (2018).

28 Ware, J. S., Samocha, K. E., Homsy, J. & Daly, M. J. Interpreting de novo Variation in Human Disease Using denovolyzeR. *Curr Protoc Hum Genet* **87**, 7 25 21-27 25 15 (2015).

29 Richards, S. *et al.* Standards and guidelines for the interpretation of sequence variants: a joint consensus recommendation of the American College of Medical Genetics and Genomics and the Association for Molecular Pathology. *Genet Med* **17**, 405-423 (2015).

30 Lonsdale, J. *et al.* The Genotype-Tissue Expression (GTEx) project. *Nat Genet* **45**, 580-585 (2013).

31 Jumper, J. *et al.* Highly accurate protein structure prediction with AlphaFold. *Nature* **596**, 583-589 (2021).

32 Yoon, W. J. *et al.* The Boston-type craniosynostosis mutation MSX2 (P148H) results in enhanced susceptibility of MSX2 to ubiquitin-dependent degradation. *J Biol Chem* **283**, 32751-32761 (2008).

33 Sarel-Gallily, R., Golan-Lev, T., Yilmaz, A., Sagi, I. & Benvenisty, N. Genome-wide analysis of haploinsufficiency in human embryonic stem cells. *Cell Rep* **38**, 110573 (2022).

34 Schwerd, T. *et al.* A biallelic mutation in IL6ST encoding the GP130 co-receptor causes immunodeficiency and craniosynostosis. *J Exp Med* **214**, 2547-2562 (2017).

35 Wuelling, M. *et al.* Trps1, a regulator of chondrocyte proliferation and differentiation, interacts with the activator form of Gli3. *Dev Biol* **328**, 40-53 (2009).

36 Veistinen, L. K. *et al.* Regulation of Calvarial Osteogenesis by Concomitant De-repression of GLI3 and Activation of IHH Targets. *Front Physiol* **8**, 1036 (2017).

37 Schwerd, T. *et al.* A variant in IL6ST with a selective IL-11 signaling defect in human and mouse. *Bone Res* **8**, 24 (2020).

38 Nieminen, P. *et al.* Inactivation of IL11 signaling causes craniosynostosis, delayed tooth eruption, and supernumerary teeth. *Am J Hum Genet* **89**, 67-81 (2011).

39 Mukherjee, A. & Rotwein, P. Selective signaling by Akt1 controls osteoblast differentiation and osteoblast-mediated osteoclast development. *Mol Cell Biol* **32**, 490-500 (2012).

ABSTRACT(IN KOREAN)

## 두개골 조기 유합증에서 TRPS1 및 IL6ST의 이인자 유전과 관련된 분자 메커니즘에 대한 분석

두개골 유합증은 생후 각 두개골의 봉합선이 합쳐 하나의 두개골을 형성하는 과정에서 정해진 시기보다 조기 유합되면서 골화가 빠르게 진행되는 경우에 발생하는 질환으로 소아에서 2,500명 당 한명의 비율로 발생하는 희귀적 질환에 해당한다. 관련하여 여러 단일 원인의 유전자가 보고되었지만 그 이외의 영역에서의 CRS의 유전적 요인은 아직 제대로 이해되지 않은 상태이다.

본 연구에서는 52쌍을 포함한 121명의 CRS 환자의 엑솜 데이터를 사용하여 드노버 변이(De novo variants)을 확인하고 반수체 부족(Haploinsufficiency)을 기반으로 이인자 유전 조합에 대한 통합 분석을 수행하였다. 연구 결과, 후보 유전자들은 골격 및 신경 발달 장애와 관련된 유전자와 분자 네트워크를 공유하며, 반수체 부족(Haploinsufficiency) 변이가 풍부하다는 사실이 확인하였다.

우리는 CRS 환자에 반수체 부족 변이군에서 2명의 환아에서 동시에 나타나는 6개의 고유한 이인자 유전(Digenic inheritance) 쌍을 확인하였고, 이 쌍에서 골화 과정과 연관성이 제일 높은 TRPS1과 IL6ST을 선택하여 세포 실험을 통해 확인된 변이의 기능적 영향을 검증하였고, 조골 세포에서의 IL6ST 및 TRPS1의 이 인자 효과로 인한 골 무기질화 가속화를 입증하였다.

이 연구는 희귀 변이 분석에서 반수체 부족(haploinsufficiency)을 기반으로 한 해석의 역할을 강조하고 CRS 발병 기전에서 이 인자 및 다인자 유전 기전으로의 확대의 필요성을 강조하는 연구가 될 것이라 사료된다.

---

핵심되는 말 : 두개골조기유합증, 이인자 유전, TRPS1, IL6ST